WHOI-2005-08

2004 Program of Study: Tides

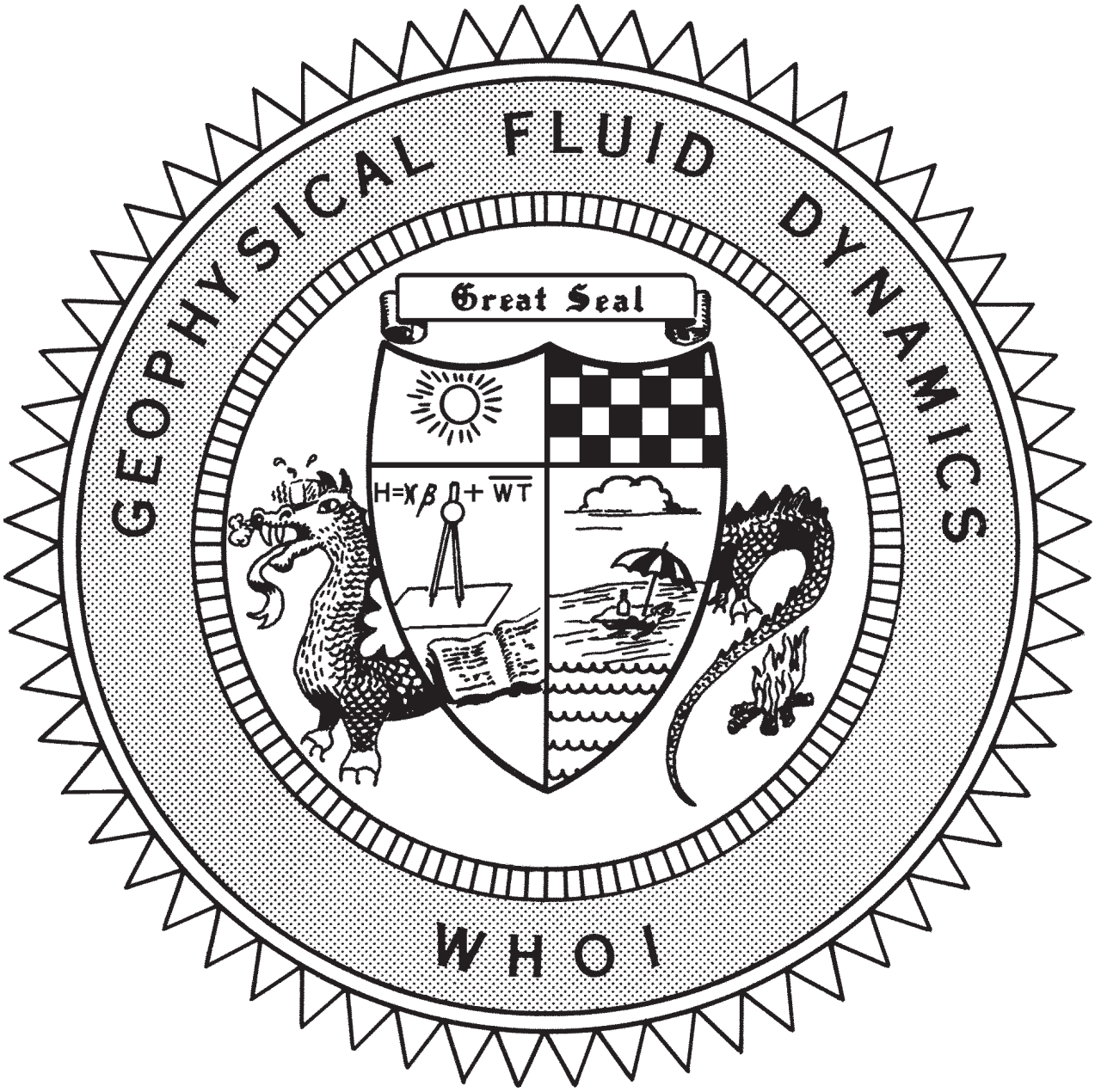

Course Lectures
Fellows Project Reports

WHOI-2005-08

2004 Program of Study: Tides

by

Neil J. Balmforth and Stefan Llewellyn-Smith Co-Directors;
Myrl Hendershott and Christopher Garrett, Principal Lecturers

July 2005

Technical Report

Funding was provided by the Office of Naval Research under Contract No. N00014-04-1-0157 and the National Science Foundation under Grant No. OCE-0325296.

Approved for Distribution:

Kenneth W. Brink for Nelson Hogg

Nelson G. Hogg, Chair

Department of Physical Oceanography

Abstract

The summer of 2004 saw the GFD program tackle “Tides”. Myrl Hendershott (Scripps Institution of Oceanography) gave a fabulous introduction to the subject in the first week of the course, laying the foundations from astronomy and classical geophysical fluid dynamics. In the second week, Chris Garrett (University of Victoria) admirably followed up with recent developments on the subject, including the recent observations from satellite altimetry, their implications to mixing and circulation, and even a memorable lecture on the noble theme of how we might solve the world's energy crisis. The principal lectures proved unusually popular this summer, and the seminar room at Walsh often overflowed in the first two weeks.

Following on from the lectures, the seminar schedule of the summer covered in greater detail the oceanographic issues with which researchers are actively grappling. We also heard about related problems regarding atmospheric, planetary and stellar tides, together with the usual mix of topics on GFD in general.

The summer once again featured a lecture for the general public in the Woods Hole area. Carl Wunsch delivered a very well received lecture entitled “Climate Change Stories”, in which he gave an impression of how scientists generally believe our climate is currently changing, whilst simultaneously urging caution against some of the more outrageous and exaggerated claims. The lecture was held at Lilly Auditorium, thanks to the hospitality of the Marine Biology Laboratory. The reception following the lecture was enjoyed by all.

Neil Balmforth and Stefan Llewellyn Smith acted as Co-Directors for the summer. Janet Fields, Jeanne Fleming and Penny Foster provided the administrative backbone to the Program, both during the summer and throughout the year beforehand. As always, we were grateful to the Woods Hole Oceanographic Institution for the use of Walsh Cottage, and Keith Bradley's solid service could not be overlooked. Shilpa Ghadge and Shreyas Mandre are to be thanked for their part in comforting the fellows, developing the summer's proceedings volume (available on the GFD web site) and for running the computer network.

TABLE OF CONTENTS

Lecture 1: Introduction to ocean tides

Myrl Hendershott

1 Introduction

The phenomenon of oceanic tides has been observed and studied by humanity for centuries. Success in localized tidal prediction and in the general understanding of tidal propagation in ocean basins led to the belief that this was a well understood phenomenon and no longer of interest for scientific investigation. However, recent decades have seen a renewal of interest for this subject by the scientific community. The goal is now to understand the dissipation of tidal energy in the ocean. Research done in the seventies suggested that rather than being mostly dissipated on continental shelves and shallow seas, tidal energy could excite far traveling internal waves in the ocean. Through interaction with oceanic currents, topographic features or with other waves, these could transfer energy to smaller scales and contribute to oceanic mixing. This has been suggested as a possible driving mechanism for the thermohaline circulation.

This first lecture is introductory and its aim is to review the tidal generating mechanisms and to arrive at a mathematical expression for the tide generating potential.

2 Tide Generating Forces

Tidal oscillations are the response of the ocean and the Earth to the gravitational pull of celestial bodies other than the Earth. Because of their movement relative to the Earth, this gravitational pull changes in time, and because of the finite size of the Earth, it also varies in space over its surface. Fortunately for local tidal prediction, the temporal response of the ocean is very linear, allowing tidal records to be interpreted as the superposition of periodic components with frequencies associated with the movements of the celestial bodies exerting the force. Spatial response is influenced by the presence of continents and bottom topography, and is a less well established matter.

Figure 1 shows a two month tidal record from Port Adelaide, Australia. Even though tidal records vary significantly for different coastal locations, this one in particular can be considered typical in that it clearly shows characteristics of tidal oscillations that can be directly related to astronomical forcings.

Perhaps the first feature to stand out is the semi-diurnal component, two high tides can be seen to occur on each day. A closer look reveals a modulation of the amplitude of the semi-diurnal oscillation, roughly over a one month period. Intervals of high amplitude are known as spring tides while those of lower amplitudes are known as neap tides. As indicated in the figure, the springs-neaps cycle is associated with the phases of the Moon. For a same day, there is often a difference in the amplitude of the two high tides. This is known as the

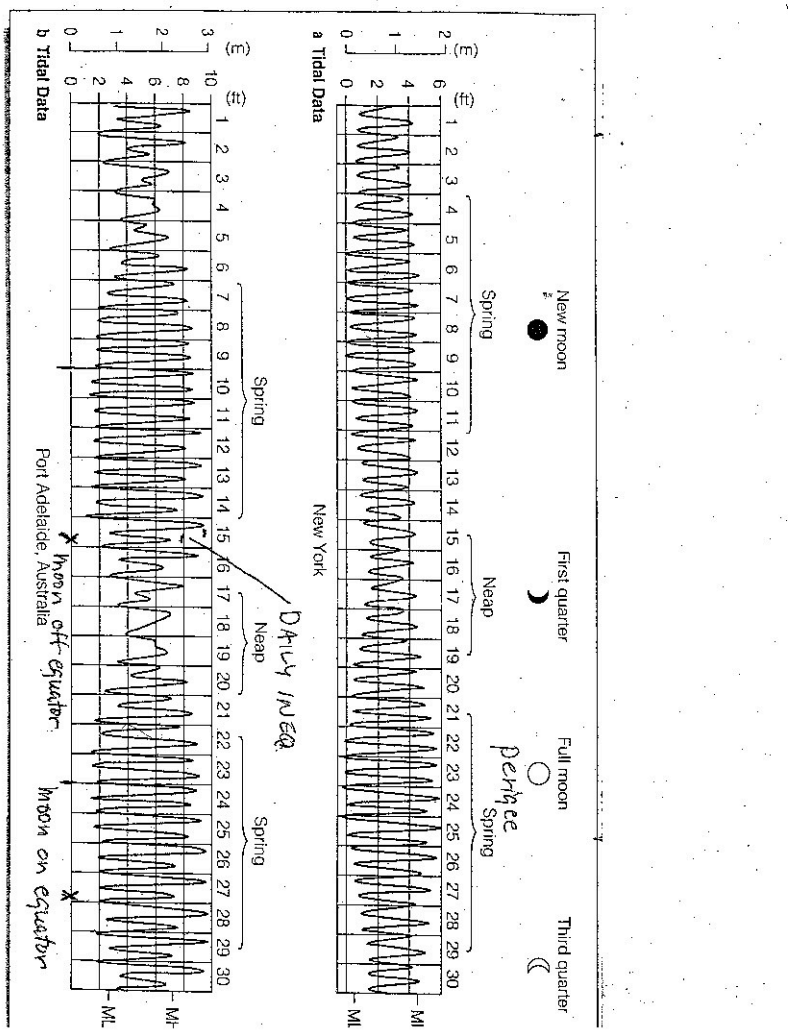

Figure 1: Two months of tidal data for Port Adelaide Australia. We can see in this record some features that can be directly accounted for by the details of the astronomical tidal forcing, such as the springs-neaps cycle, the daily inequality and the absence of daily inequality when the Moon is on the Equator.

"daily inequality" and, as indicated in the figure, disappears when the Moon is over the equator.

We will try to clarify below the basic ideas underlying tidal forcing. We will also try to explain the origin of the forcing terms responsible for causing the tidal record features described above. Finally we will attempt to explain the derivation of the tide generating potential.

3 Tidal Forcing

Even though small compared to the planets and especially to the sun, the Moon is by far the celestial body closest to the Earth. Because gravitational pull decreases linearly with mass and quadratically with distance, the Moon exerts the biggest influence over the Earth, contributing the most to the formation of tides. We will begin by considering its effects.

The centres of mass of the Earth and the Moon orbit around the common centre of mass of the Earth-Moon system. Their movements are such that centrifugal force counterbalances gravitational attraction at the individual centres of mass. The Earth is a rigid body, so every material point in it executes an identical orbit, and is therefore subject to the same centrifugal force, as illustrated in figure 2. Gravitational force however will vary because the distance between these points to the Moon may vary by up to one Earth diameter. Gravitational force will prevail over centrifugal force on the hemisphere closest to the Moon and centrifugal force will prevail on the hemisphere furthest to it. The opposite hemispheres have net forces in opposite directions, causing the ocean to bulge on both sides. As the Earth spins under this configuration, two daily tides are felt.

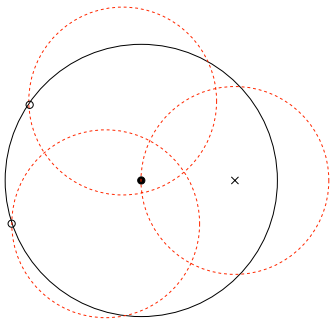

Figure 2: The centre of the Earth, shown as a filled dot, rotates about the centre of mass of the Earth-Moon system, indicated by a 'x' mark. Dashed circles show the orbital movement of the points shown by a 'o' mark on Earth's surface and the center of the Earth.

A common source of confusion regarding the argument above is to suppose that the centrifugal force relevant to the problem is due to the spinning of the Earth around its own axis. This seems reasonable at first sight because this force is constant for every latitude circle, allowing for an imbalance with lunar attraction, which is longitude dependent at any given instant. However, the centrifugal force due to the Earth's spin has permanently deformed the Earth's surface into a spheroid (as opposed to the spherical shape that would ensue from self-gravitation only). That is to say, this centrifugal force is compensated by

the Earth's own gravitational field. A mnemonic phrase to keep in mind is that tides are caused by the action of *other* celestial bodies over the Earth.

Another not entirely uncommon misconception is that tides are partly the result of the variation of centrifugal force over the surface of the Earth. This kind of confusion arises because the distance between the centre of the Earth-Moon system is smaller than one Earth radius and therefore this point lies "within" the Earth. If this were a fixed material point, like the centre of the Earth, around which the planet revolved, there would indeed be a variation of centrifugal force with distance from it. However, the centre of mass of the Earth-Moon system is just a point in space, and as the Earth revolves around it, as indicated in figure 2 none of its material points are fixed.

Even though a constant field, the centrifugal force due to the revolution of the Earth around the system's centre of mass is essential to the semi-diurnality of the tides. We can illustrate this by considering the situation in which the centre of the Earth is fixed. In this case the only force acting upon it is lunar gravitational attraction. Although uneven over the surface, it pulls every point on Earth towards the Moon, causing the water to bulge on the hemisphere closer to it. The spinning of the Earth would therefore make every point on it experience a diurnal tide cycle, instead of a semi-diurnal one. This situation is illustrated in figure 3

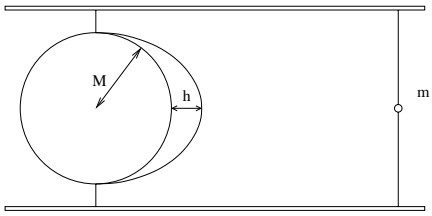

Figure 3: Tidal deformation that would ensue if from lunar attraction if the Earth's centre of mass were fixed.

We can calculate the surface elevation that would result from this forcing. The assumption is that the elevation would be such that net terrestrial gravitational force would exactly compensate for the lunar force at the point.

Net Moon's gravitational force:

$$\frac{GM}{(a+h)^2} - \frac{GM}{a^2} \simeq -\frac{GM}{a^2}\frac{2h}{a}.$$

Net Earth's gravitational force:

$$\frac{GM}{a^2}(\frac{a}{r})^2\frac{m}{M},$$

where M is the mass of the Earth, r is the distance between Earth's and Moon's centres of mass, a is the Earth's radius, h is the sea surface deformation at the sub lunar point and G is the universal gravitational constant. Equating the two forces and isolating h we get:

$$h = \frac{a^3}{2r^2}\frac{m}{M} = 10.7\text{m}. \tag{1}$$

This is an unrealistically high value.

If we now allow the Earth's centre of mass to accelerate, the centrifugal force due to this motion will compensate for the Moon's gravity at that point. We can anticipate that tidal deformation will be smaller, since it will be a response to a smaller resultant force. As explained earlier, predominance of lunar attraction on the hemisphere facing the Moon and of the centrifugal force on the one opposing deforms the surface into an ellipsoid. The water will bulge around the sub-lunar and anti-sub lunar points.

For this case we can also calculate tidal elevation on the sub-lunar point.

$$\frac{Gm}{(r-a)^2} - \frac{Gm}{r^2} \simeq \frac{GM}{r^2}\frac{2a}{r}, \tag{2}$$

where the first term on the right is lunar gravity, the second is the centrifugal force and the term on the right is the net gravitational force of the Earth. Isolating h we get:

$$h = \frac{a^4}{r^3}\frac{m}{M} = 35.8\text{cm} \tag{3}$$

The Moon rotates around the Earth in the same direction as the Earth spins, and the surface deformation must rotate with it. It takes slightly longer than a day for the Moon to be directly over the same point on the Earth's surface, as illustrated in figure 4 this is called a lunar day. Likewise, the period between two high tides is half lunar day. Apart from the semi-diurnal tides, we can expect the presence of the Moon to permanently deform the sea surface. This is an order zero effect called the permanent tide.

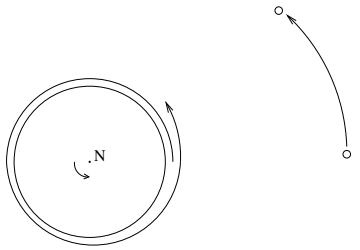

Figure 4: The Earth-Moon system. The position of the Moon with respect to a fixed point on the Earth's surface after one revolution is illustrated.

Up to now, we have considered the orbit of the Moon circular. It is however elliptic, with the Earth-Moon centre of mass being one of the foci. The Moon's gravitational force over the Earth will be modulated over the period of one anomalistic month (figure 5), as will the tidal components it generates.

In summary, tidal forcing by the Moon alone can be represented by the following harmonics:

Lunar Semi-Diurnal Tide (M_2) $2/LD$	12h 25.236 min
Lunar Elliptical (N_2)	$2/LD - 1/perigee$ 12h 3.501 min
Lunar Monthly Elliptical (M_m)	$1/perigee$ 27.5545 days (anomalistic month)

The $2/LD + 1/perigee$ term was left out because it has a small amplitude. Modulation of the amplitude of M_2 is represented by the interaction of M_2 and N_2, which is constructive once each anomalistic month.

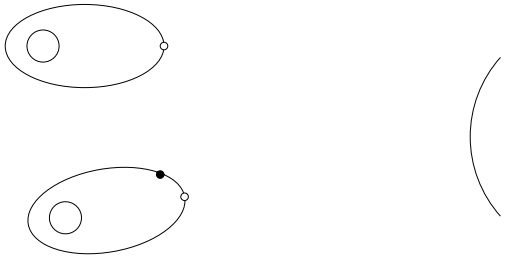

Figure 5: As the Moon rotates around the Earth, the Earth rotates around the Sun. For this reason, after each orbital period (anomalistic month), the Moon is in different position in its orbit with respect to the Sun. In the above picture, we represent on top an initial position of the Earth and Moon, below it their position after one anomalistic month. The black Moon in this case represents the position it would have to be in to exhibit the same phase as in the initial configuration.

All arguments mentioned above are valid for any other celestial body which might be reasonably considered to form a two body system with the Earth, for which the orbits are elliptical. Another such body is the sun, whose tidal effect over the Earth (when the two body system is considered in isolation) can be reduced to the harmonic components below.

Solar Semi-Diurnal Tide (S_2)	$2/SD$ 12h 25.236 min
Solar Elliptical (N_2)	$2/SD - 1/anom.yr.$ 12h 3.501 min
Solar Annual Elliptical ()	$1/perihelion$ 365.25964 days (anomalistic year)

When Moon and Sun are aligned with the Earth, their semi-diurnal components interfere constructively, giving rise to tides of larger amplitude, known as spring tides. When they are in quadrature, the interference is exactly destructive, giving rise to smaller amplitude tidal variations, called neap tides. The relative arrangement of the Earth Sun and Moon is perceived on the Earth as the phases of the Moon, and therefore the springs-neaps cycle has a period of one lunar (synodic) month. A lunar month is the duration required for the Moon to return to a fixed position in its orbit in relation to the Sun as illustrated in figure 5.

Up to now we have assumed that the orbits of the Earth (around the Sun) and Moon are coplanar to the spinning of the Earth at all instants of time. In reality these planes intersect at an angle. The effect this has over the tide is illustrated in figure 6. As the Earth rotates,

it perceives the tidal surface as being "tilted" in relation to latitude. In terms of harmonics, this is represented by a daily component, which gives rise to the daily inequality. When the tide generating bodies intersect the equatorial plane, the daily inequality disappears. In the Port Adelaide record (figure 1), we can see that daily inequality disappears when the Moon is on the Equator.

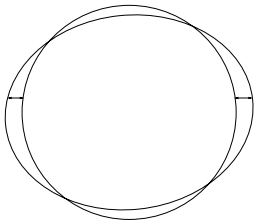

Figure 6: The Moon's orbit is not coplanar with the Equator. The tidal surface is in general "tilted" with respect to the Equator giving rise to the daily inequality.

The amplitude of the declinational components depends on the angle of the bodies orbit to the equatorial plane. Both the lunar orbital plane and the ecliptic precess, modulating the declinational tides. The Moon's orbit precesses over 18.6 years, its angle to the Ecliptic varying between $-5°08'$ and $5°08'$. In relation to the Earth's equatorial plane the variation is between $23°27' - 5°08'$ and $23°27' + 5°08'$.

As mentioned earlier, the usefulness of decomposing the tide generating force into harmonics is due to the linearity of the oceans response to it in time. In fact, we have taken this for granted in the preceding section when we explained the springs-neaps cycle purely as the result of the interference of two forcing terms. This property allows for more precise tidal prediction. Tidal records are not used to determine the important frequencies in their harmonic expansions, these are known from astronomical considerations. Data is used only to determine the amplitudes of local response to these terms.

4 Spatial Structure of the Tides

As the Earth's spinning under the tide generating potential is felt as the propagation of the tidal wave. However, this propagation is obstructed by the presence of continents and bottom topography. Real co-tidal lines therefore look nothing like the constant phase lines of the tide generating potential. As a plane wave enters a basin, it feels the effect of the Earth's rotation and propagates along its borders. The nodal line that would exist in the case with no rotation degenerates into a nodal point, called amphidromic point.The irregularity of the oceanic basins and of bottom topography disrupt the propagation and a precise map of tidal propagation could only be obtained after the advent of satellite altimetry. This data is harmonically analyzed to obtain maps for the different astronomical components. Figure 7 shows a co-tidal map obtained in this manner. Although the amphidromic points are eye catching, the less conspicuous anti-amphidromic points, for which tidal amplitude is maximum and there is almost no phase variation, are probably more useful for testing satellite altimetry.

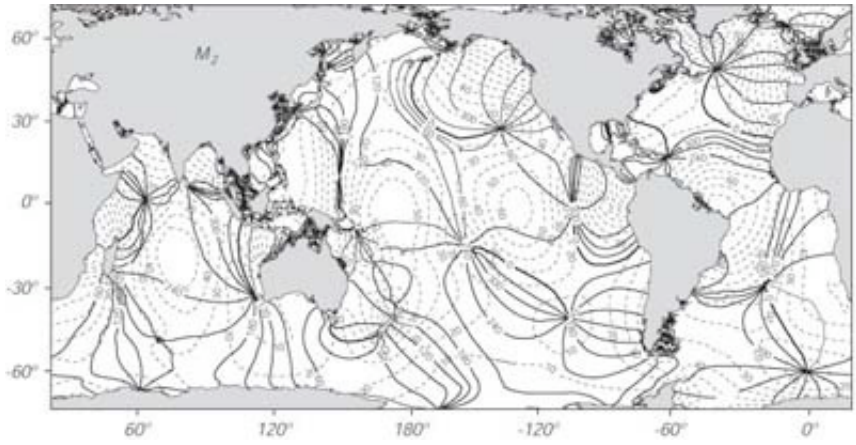

Figure 7: Cotidal map. Amphidromic points are the ones where cotidal lines cross. In these points tidal amplitude is zero and phase speed infinite. Less conspicuous are the anti-amphidromic points, where tidal amplitude is maximum and phase stationary.

In the following section we will formalize the ideas outlined above so as to arrive at an expression for the tide generating potential.

5 The tide generating potential

We want to calculate the tidal force that the Moon or Sun exerts on the Earth, in particular on the oceans. Remember that we are only interested in the effects of *another* body on the Earth, not the effect of the Earth's rotation and gravity on its shape and that of the oceans.

Consider the plane made up of the centre of the Earth, the tide generating body (the Moon or the Sun), assumed to be a point mass, and an observer at P on the surface of the Earth, as shown in figure 8. For the moment, we assume R is constant.

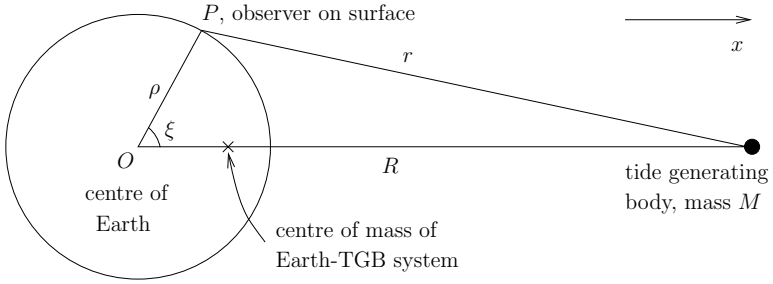

Figure 8: The geometry for calculating the tidal force at P due to the tide generating body.

The tide generating body (TGB) exerts a force, $\mathbf{F}$, on the centre of the Earth

$$\mathbf{F} = \frac{GM}{R^2}\,\hat{\imath},$$

where $\hat{\imath}$ is the unit normal along the x-direction and G is the universal gravitational constant. From this, the potential at the centre of the Earth, O, due to the TGB is

$$V(O) = \frac{GM}{R^2}\, x + \text{const} = \frac{GM}{R^2}\rho\cos\xi + \text{const},$$

where the constant is arbitrary.

Then the resultant force at P is the gravitational force at P, less that at O, with potential

$$V(P) = \frac{GM}{r} - \frac{GM}{R^2}\rho\cos\xi. \tag{4}$$

The sign is chosen as r is measured away from the TGB and the force should be towards it. Note that the force on the Earth as a whole, $\mathbf{F}$, is balanced by the centrifugal force due to the motion of the Earth about the common centre of mass of the Earth–TGB system.

The parameters r, R, ρ and ξ are linked by $r^2 = R^2 - 2\rho R\cos\xi + \rho^2$ from properties of triangles. Hence

$$\frac{1}{r} = \frac{1}{R}\left(1 - \frac{2\rho}{R}\cos\xi + \frac{\rho^2}{R^2}\right)^{-\frac{1}{2}} = \frac{1}{R}\sum_{n=0}^{\infty}\left(\frac{\rho}{R}\right)^n P_n(\cos\xi), \tag{5}$$

where $P_n(z)$ is the nth Legendre polynomial, with $P_0(z) = 1$, $P_1(z) = z$, $P_2(z) = (3z^2-1)/2$, ... The final equality in (5) may be found in, for example, Morse and Feshbach [1].

Hence (4) becomes

$$V(P) = \frac{GM}{R}\left[1 + \sum_{n=2}^{\infty}\left(\frac{\rho}{R}\right)^n P_n(\cos\xi)\right].$$

For the Moon, $0.0157 \le \rho/R \le 0.0180$ and for the Sun $\rho/R \sim 10^{-4}$. Hence the potential may be truncated at $n = 2$. Forgetting about the constant GM/R, which is unimportant since ultimately we want to find the forces, it becomes

$$V(P) \simeq \frac{GM}{R}\left(\frac{\rho}{R}\right)^2 P_2(\cos\xi). \tag{6}$$

Note that this potential is symmetric in ξ. This is consistent with the discussion in previous sections, where we argued that the tide generating force is symmetrical with respect to the plane that contains the Earth's centre of mass and is orthogonal to the Earth-Moon axis.

5.1 The tide generating potential in geographical coordinates

It is more useful to express the tidal potential in geographical coordinates: actual latitude and longitude of the observer on the Earth and the apparent latitude and longitude of the TGB. This coordinate system is shown in figure 9. We call attention to the fact that the longitudinal angles are measures with respect to the Equator. In this coordinate system the tidal ellipsoid is "tilted", and the tidal potential will therefore have asymmetrical components.

From spherical trigonometry

$$\cos\xi = \sin\theta\sin\delta + \cos\theta\cos\delta\cos H.$$

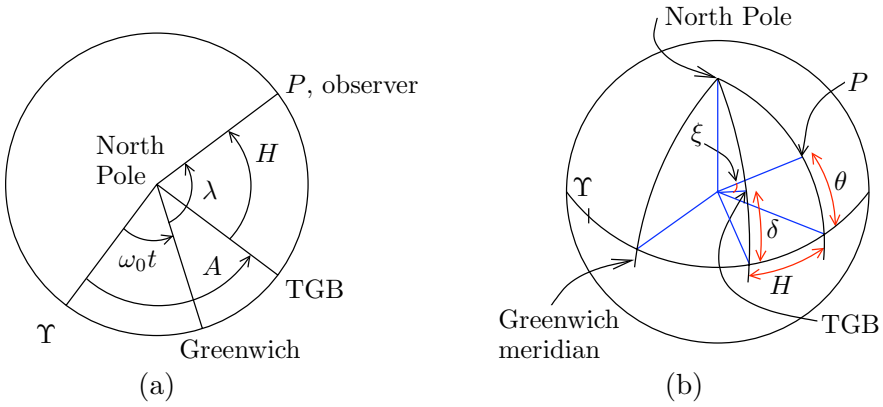

Figure 9: The geographical coordinates: (a) looking down from the North Pole and (b) looking at the spherical Earth. Here λ is the geographic longitude of the observer and θ is the geographic latitude. ξ is the angle between the TGB and the observer as in figure 8. δ is the *declination* of the TGB and A is the *right ascension* of the TGB, or its apparent longitude with respect to an origin Υ. Υ is a celestial reference point from which to measure positions of the TGB: it is the northward crossing of the Sun at equinox, or equivalently the point of intersection of the equatorial plane and the *ecliptic*, the plane of the Earth's orbit about the Sun, as the Sun travels northward. The point Υ is assumed fixed with respect to the fixed stars for the current discussion. However, with respect to the rotating Earth, the point Υ moves. If $t = 0$ is taken to be the time at which Υ lies on the Greenwich meridian, then at time t, the Earth has rotated $\omega_0 t$ giving the angle between Υ and Greenwich, where ω_0 is the frequency associated with the period of rotation of the Earth about its axis so that the TGB appears again in the same Earth–TGB orientation. $H = \omega_0 t + \lambda - A$ is referred to as the hour angle.

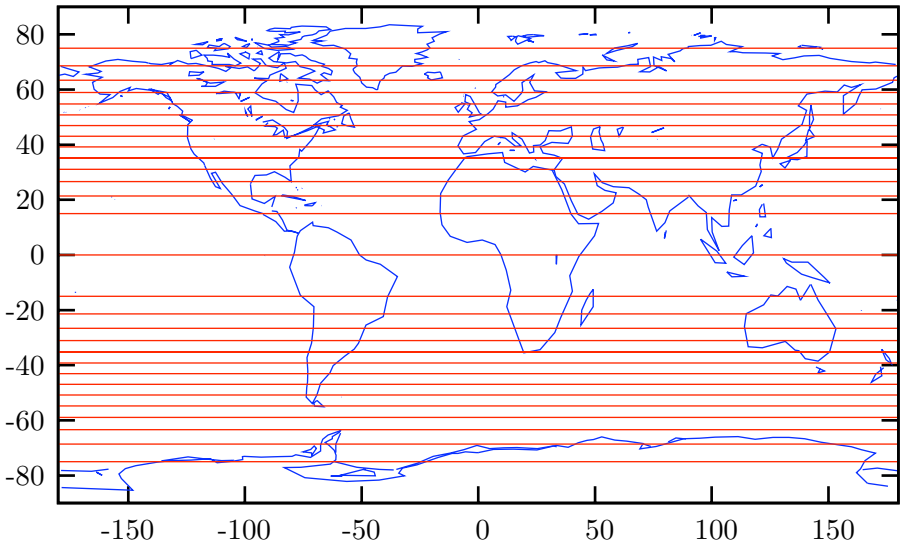

Figure 10: Equipotential lines for the long-period potential.

Substituting this in (6) gives

$$V(\lambda,\theta) \simeq \frac{3GM\rho^2}{4R_0^3}\left(\frac{R_0}{R}\right)^3\left[\frac{4}{3}\left(\frac{1}{2}-\frac{3}{2}\sin^2\theta\right)\left(\frac{1}{2}-\frac{3}{2}\sin^2\delta\right)\right.$$
$$\left.+\sin 2\theta\sin 2\delta\cos H+\cos^2\theta\cos^2\delta\cos 2H\right], \qquad (7)$$

where R_0 is a reference value of the orbital distance R of the TGB. The coefficient $3GM\rho^2/4R_0^3$ is referred to as the *Doodson constant*, D. For the Moon, $D_{\text{Moon}}/g = 26.75\,\text{cm}$ and for the Sun, $D_{\text{sun}} = 0.4605 D_{\text{Moon}}$.

The first term in the square bracket in (7) has no dependence on the hour angle, H, and gives rise to a long-period[1] potential. The second term gives rise to a diurnal potential and the final term to a semi-diurnal potential. Figures 10-12 show plots of the instantaneous equipotential lines for the three components of (7) and plots of the cotidal[2] and corange[3] lines. The plots shown are in fact representative of the solid Earth tide, since the response time of the Earth is of the order of an hour (deduced from earthquake measurements), much quicker than the time period of the tidal potential and so the solid Earth can adjust to the equipotential surfaces. The oceans have a much longer response time.

In reality, the declination and orbital distance in (7) vary in time. In the following sections, we consider how these variations change the potential.

[1] In the present analysis, infinitely long. However we shall see that each term of the potential is modulated and hence this becomes a long-period potential.

[2] A line passing through points at which high tide occurs at the same number of hours after the Moon transits the Greenwich meridian.

[3] A line passing through points of equal tidal range.

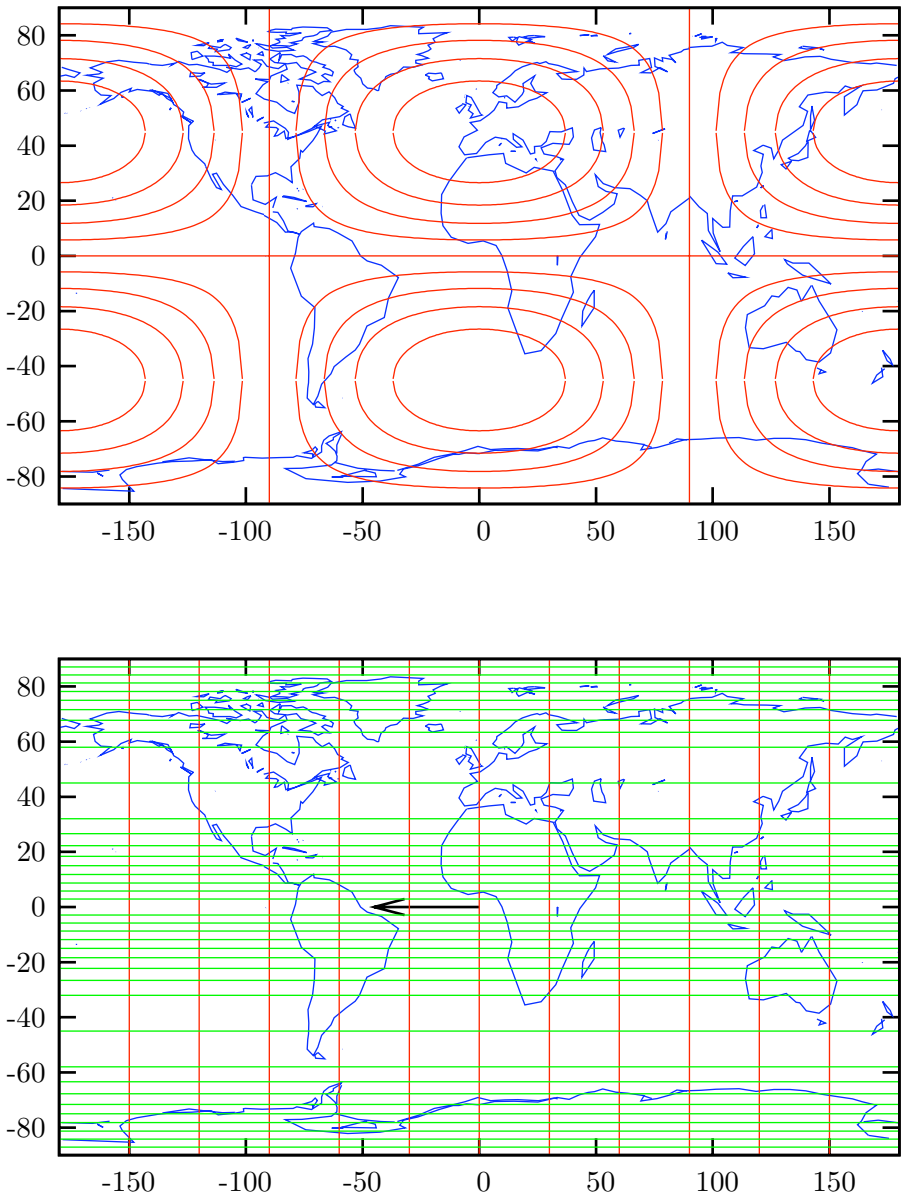

Figure 11: Equipotential lines (top) and cotidal, green, and corange, red, lines (bottom) for the diurnal potential.The arrow indicates the direction of increasing cotidal time.

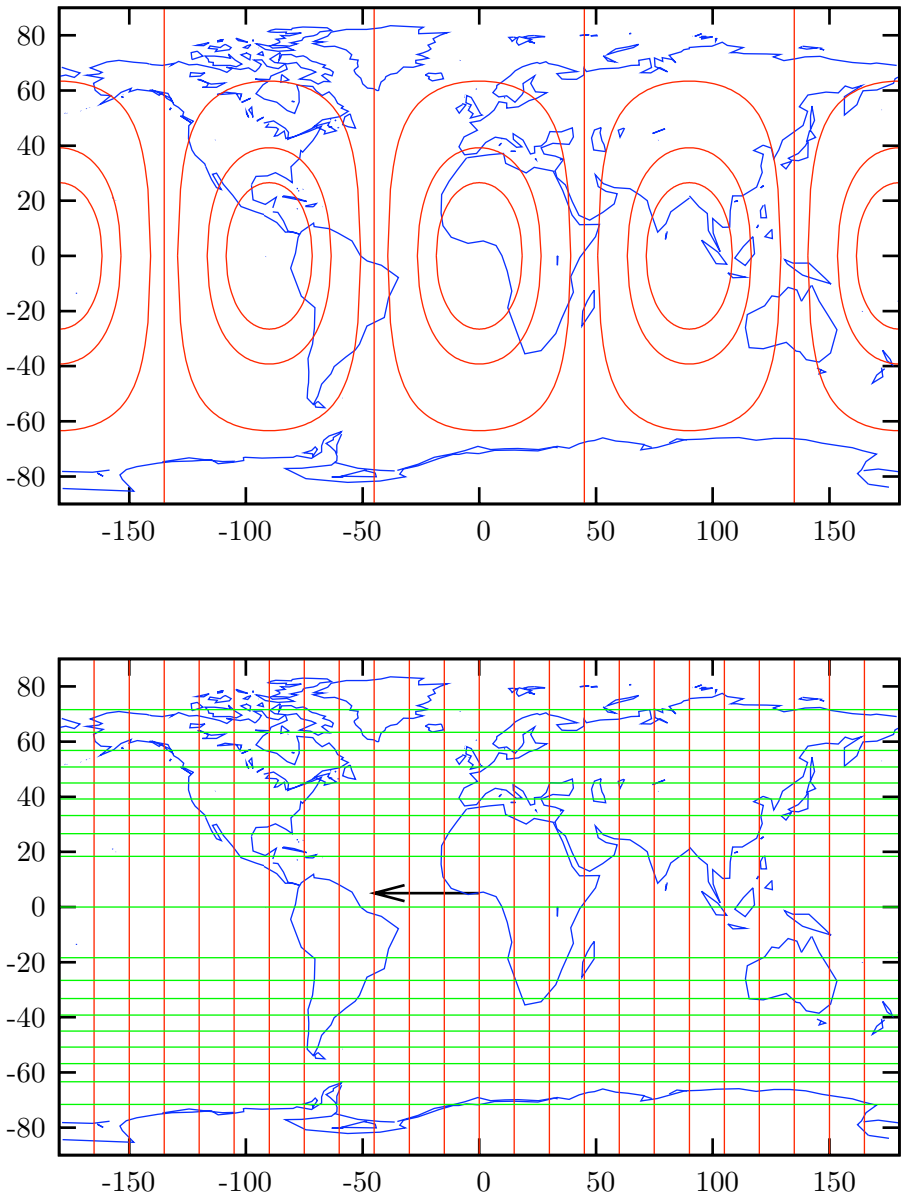

Figure 12: Equipotential lines (top) and cotidal, green, and corange, red, lines (bottom) for the semi-diurnal potential. The arrow indicates the direction of increasing cotidal time.

5.2 Variation of the declination of the tide generating body

The angle δ in figure 9b and (7) varies in time, based on the location of the tide generating body relative to the plane of the equator. This variation has a time period related to the precession of the equinoxes for the Sun and to the precession of the lunar node for the Moon.

5.2.1 Precession of the equinoxes

The Earth's rotational axis is tilted, at present at $24°27'$, to the ecliptic.[4] As the Earth rotates about the Sun, this means that the declination of the Sun varies, as shown in figure 13a. Hence only after a 'year' is the declination expected to return to its initial value.

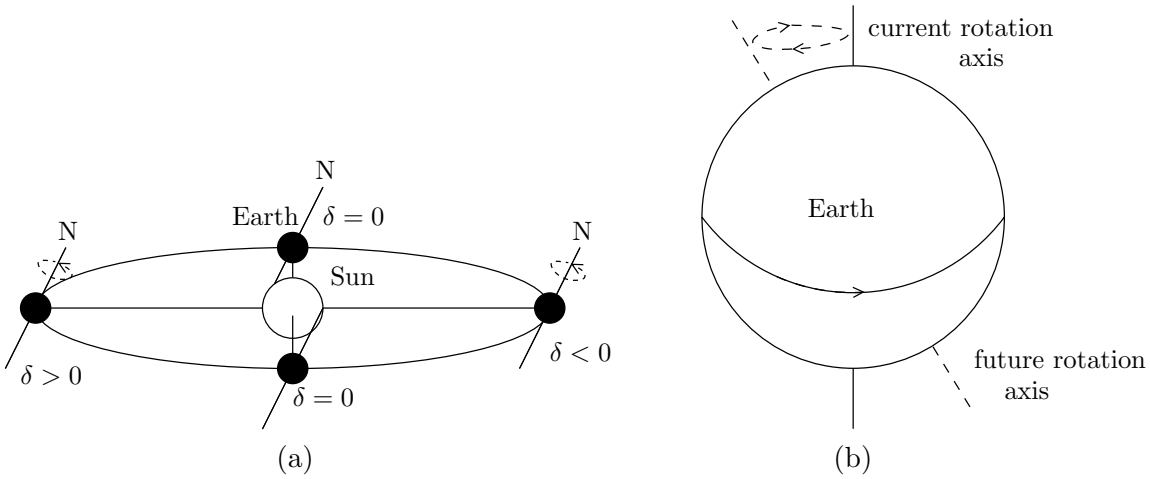

Figure 13: (a) The variation in declination due to the rotation of the Earth about the Sun. (b) The precession of the equinoxes.

Lunar and solar gravity act on the oblate Earth, making it spin like a top, with its rotation axis precessing as depicted in figure 13b. The celestial point where the Sun crosses the plane of the equator, moving from south to north is known as the *Point of Aries* or the vernal equinox and is the point Υ in figure 9 at which $\delta = 0$. Due to precession, it moves eastward relative to the fixed stars.[5] The period of precession is 25570 years. The time period of the revolution of the Earth about the Sun from vernal equinox to vernal equinox is the tropical year and is 365.242199 mean solar days. This is the 'year' we are interested in for the declination returning to its original value.

5.2.2 Precession of the lunar node

The plane of the Moon's orbit around the Earth is inclined at $5°08'$ with respect to the ecliptic. It precesses with a period of 18613 years due to the Earth's gravity.

[4] The plane of the Earth's orbit around the Sun.

[5] In antiquity, it *was* in the constellation Aries. Now it is in Pisces.

The intersection of the plane of the Moon's orbit with the equatorial plane as the Moon goes from south to north is the *ascending lunar node*, Ω. The mean time period separating adjacent passages through Ω is the tropical month of 27.321582 mean solar days. This is the time period before the same declination of the Moon is again achieved.

5.3 Variation of the orbital distance of the TGB

In reality, R is not fixed in (7), since the Moon and Sun are not a constant distance from the Earth. Here we consider how the orbital distance of the Moon varies in time. The same analysis also applied for the Sun.

5.3.1 Kepler's laws

The orbit of the Moon about the Earth is an ellipse (Kepler's first law), as we now show. Consider the geometry shown in figure 14. From Newton's laws,

$$m\ddot{\mathbf{x}} = -GmM\mathbf{x}/R^3,$$

where $\mathbf{x}$ is the position vector of the Moon relative to the Earth.

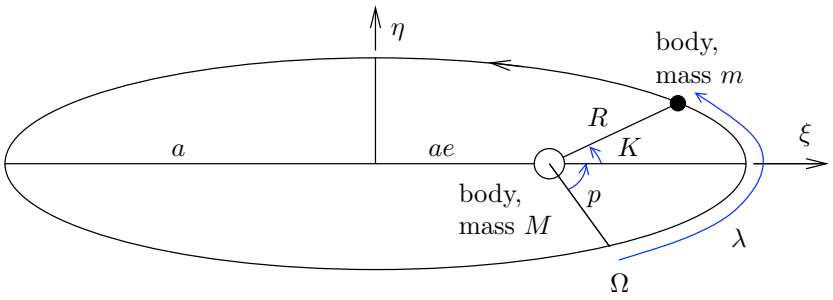

Figure 14: The Moon of mass m in orbit about the Earth of mass M. Assume that the Earth is fixed in space.

Rewriting this equation in polar coordinates, with $x = R\cos\lambda_e$ and $y = R\sin\lambda_e$ gives

$$\ddot{R} - R\dot{\lambda_e}^2 = -GM/R^2, \qquad R\ddot{\lambda_e} + 2\dot{R}\dot{\lambda_e} = 0.$$

Integrating the second equation gives Kepler's second law

$$R^2\dot{\lambda_e} = \text{constant} = h, \tag{8}$$

which says that the line joining the orbiting Moon and the Earth sweeps out equal areas in equal intervals of time. Integrating the first equation, by setting $u = 1/R$, gives

$$\frac{1}{R} = A'\cos K + \frac{GM}{h^2}, \tag{9}$$

where A' is a constant of integration and we have used the fact that $1/R$ is symmetric about the line $\eta = 0$. This is the equation of an ellipse with semi-major axis a and eccentricity e satisfying $A' = e/a(1-e^2)$ and $gM/h^2 = 1/a(1-e^2)$.

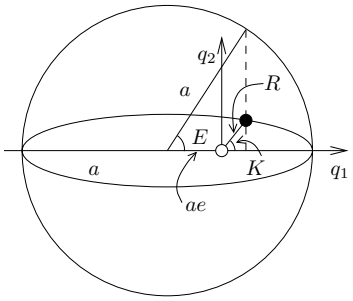

Figure 15: The definition of the eccentric anomaly E.

We now want to see how this modifies the potential given in (7). Instead of using the *true anomaly*, K, it is more useful to write (9) in terms of the *eccentric anomaly*, E, defined as shown in figure 15. Then it is possible to write

$$R = a(1 - e\cos E) \tag{10}$$

and the motion of the Moon in its orbit is given by *Kepler's equation*

$$E - e\sin E = \omega_k t, \tag{11}$$

in which $t = 0$ at perigee[6] and $\omega_k = \sqrt{GM/a^3}$, the *Kepler frequency*. The *mean anomaly*, E_0 is related to E by

$$E_0 = E - \sin E$$

and increases uniformly in time: $E_0 = \omega_k t$ from (11).

In (7) we then have, assuming the eccentricity e is small,

$$R_0/R \equiv a/R = (1 - e\cos E)^{-1} \sim 1 + e\cos E_0 + e^2\cos 2E_0 + \ldots,$$

from (10) and

$$R_0/R = a/R = (1 + e\cos K)/(1 - e^2),$$

from (9). Hence $K \simeq E_0 + 2e\sin E_0 + \ldots$.

Remembering from figure 14 that the *ecliptic longitude*, $\lambda_e = p + K$ and setting the *mean longitude* to be $h = p + E_0$ we obtain

$$\begin{aligned} R/R_0 &= 1 + e\cos(h - p) + e^2\cos 2(h - p) + \ldots, \\ \lambda_e &= h + 2e\sin(h - p) + \ldots. \end{aligned}$$

This can be simply translated into geographical coordinates for the Sun as the tide generating body. For the Sun

$$\sin\delta = \sin\lambda_e \sin\epsilon, \qquad A = \lambda_e - \tan^2(\epsilon/2)\sin\lambda_e,$$

[6]The point in the orbit of the Moon nearest the Earth.

where δ is the declination, λ_e is the ecliptic longitude, A is the right ascension of the Sun and ϵ is the angle between the ecliptic and the equatorial plane.

For the Earth–Moon system it is actually more complex to write the solution in terms of the geographical coordinates as the lunar node does not coincide with the point of Aries and the Moon's orbit is not in the ecliptic. Furthermore, there is a strong solar perturbation to its orbit.

5.4 Tidal harmonics

The effect of the variations of declination and distances to the tide generating bodies is to alter the coefficients for terms in (7). These variations may be Fourier decomposed and result in modulations of the basic tidal frequencies: the long-period, diurnal and semi-diurnal. Then the potential given in (7) may be written as

$$V(\lambda,\theta) = V_0(\lambda,\theta) + V_1(\lambda,\theta) + V_2(\lambda,\theta), \tag{12}$$

where

$$V_s(\lambda,\theta) = DG_s \sum_j C_j \cos(\sigma_j t + s\lambda + \theta_j)$$

with $G_0 = (1 - 3\sin^2\theta)/2$, $G_1 = \sin 2\theta$ and $G_2 = \cos^2\theta$; D the Doodson constant and C_j the amplitude of the component. The harmonic frequency σ_j is a linear combination of the angular velocity of the Earth's rotation ω [already seen in (7) in the hour angle] and the sum and the difference of angular velocities ω_k with $k = 1, \ldots, 5$ which are the five fundamental astronomical frequencies, having the largest effect modifying the potentials (it is possible to include many more). These five frequencies are given in table 1. Hence

$$\sigma_j = s\omega + \sum_{k=1}^{5} m_k^j \omega_k,$$

where $s = 0, 1, 2$ for the long-period, diurnal and semi-diurnal respectively; $m_k^j = 0, \pm 1, \pm 2, \ldots$ and ω is either taken to be $\omega_0 - \omega_1$ for the Moon as the TGB, or $\omega_0 - \omega_2$ for the Sun with ω_0 the sidereal[7] frequency. λ is the longitude of the observer.

All tidal harmonics with amplitudes $C > 0.05$ are given in table 2.

5.4.1 Doodson numbers

For convenience, the frequencies σ_j may be written as

$$\text{Doodson number} = s\, m_1^j\, m_2^j\, m_3^j\, m_4^j\, m_5^j + 0\,5\,5\,5\,5\,5,$$

where the addition of 055555 is simply so that the Doodson numbers are all positive (since in general the m_i^j lie in the range $-5 \le m_i^j < 5$). The Doodson numbers are also given in table 2.

[7]The length of time between consecutive passes of a given 'fixed' star in the sky over the Greenwich meridian. The sidereal day is 23 hr56 min, slightly shorter than the 'normal' or solar day because the Earth's orbital motion about the Sun means the Earth has to rotate slightly more than one turn with respect to the 'fixed' stars in order to reach the same Earth–Sun orientation.

Period	Nomenclature
$360^\circ/\omega_1 = 27.321582\,\text{days}$	period of lunar declination
$360^\circ/\omega_2 = 365.242199\,\text{days}$	period of solar declination
$360^\circ/\omega_3 = 8.847\,\text{years}$	period of lunar perigee rotation
$360^\circ/\omega_4 = 18.613\,\text{years}$	period of lunar node rotation
$360^\circ/\omega_5 = 20940\,\text{years}$	period of perihelion rotation

Table 1: The fundamental periods of the Earth's and the Moon's orbital motion. *From Bartels* [2].

5.4.2 Spectra of the tides

Figure 16 shows a plot of the spectrum of equilibrium tides with frequencies near twice per day (the semi-diurnal tides). The spectrum is split into groups separated by a cycle per month (0.55°hr^{-1}). Each of these is further split into groups separated by a cycle per year (0.04°hr^{-1}). The finest splitting in the figure is at a cycle per 8.847 years ($0.0046^\circ\text{hr}^{-1}$).

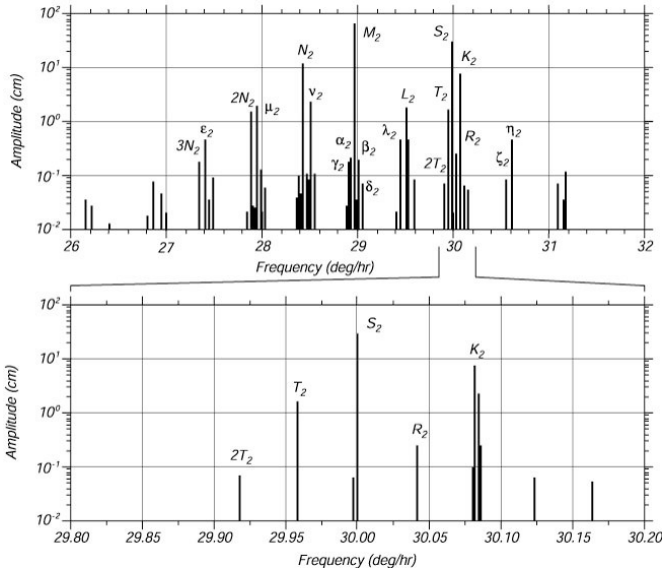

Figure 16: A spectrum for equilibrium tides. *From* `oceanworld.tamu.edu/resources/`.

Notes by Josefina Arraut and Anja Slim.

References

[1] P. M. Morse and H. Feshbach, *Methods of Theoretical Physics* (McGraw-Hill, New York, 1953).

[2] J. Bartels, *Handbuch der Physik* (Springer, Berlin, 1967), Vol. 48.

Ampl., C	Frequency, σ $^\circ\,\mathrm{hr}^{-1}$	Period $360^\circ/\sigma$	Doodson number	Notation
		Long period tides		
0.2341	0		055555	S_0 (solar constant)
0.5046	0		055555	M_0 (lunar constant)
0.0655	$\omega_4 = 0.00221$	18.613 years	055565	– (nodal M_0)
0.0729	$2\omega_2 = 0.08214$	182.621 days	057555	S_{sa} (declinational S_0)
0.0825	$\omega_1 - \omega_3 = 0.54437$	27.555 days	065455	M_m (elliptical M_0)
0.1564	$2\omega_1 = 1.09803$	13.661 days	075555	M_f (declinational M_0)
0.0648	$2\omega_1 + \omega_4 = 1.10024$	13.663 days	075565	– (nodal M_0)
		Diurnal tides		
0.0722	$\omega_(- 2\omega_1 + \omega_3 = 13.39866$	26.868	135655	Q_1 (elliptical O_1)
0.0710	$-\omega_(+ \omega_1 - \omega_4 = 13.94083$	25.823	145565	– (nodal O_1)
0.3769	$\omega_(- \omega_1 = 13.94304$	25.819	145555	O_1 (basic lunar)
0.1755	$\omega_\odot - \omega_2 = 14.95893$	24.066	163555	P_1 (basic solar)
0.1682	$\omega_\odot + \omega_2 = 15.04107$	23.934	165555	K_1^S (declinational P_1)
0.3623	$\omega_(+ \omega_1 = 15.04107$	23.934	165555	K_1^M (declinational O_1)
0.0718	$\omega_(- \omega_1 + \omega_4 = 15.04328$	23.931	145565	– (nodal K_1^M)
		Semi-diurnal tides		
0.1739	$2\omega_(- \omega_1 + \omega_3 = 28.43973$	12.658	245655	N_2 (elliptical M_2)
0.9081	$2\omega_(= 28.98410$	12.421	255555	M_2 (basic lunar)
0.4229	$2\omega_\odot = 30.00000$	12.000	273555	S_2 (basic solar)
0.0365	$2\omega_\odot + 2\omega_2 = 30.08214$	11.967	275555	K_2^S (declinational S_2)
0.0786	$2\omega_(+ 1\omega_2 = 30.08214$	11.967	275555	K_2^M (declinational M_2)
		Combined tides		
0.5305	$\omega_0 = 15.04107$	23.934		K_1 (lunar-solar declinational)
0.1151	$2\omega_0 = 30.08214$	11.967		K_2 (lunar-solar declinational)

Table 2: The tidal harmonics with amplitude coefficients $C > 0.05$. $\omega_\odot$ is $\omega_0 - \omega_2$, associated with the Sun and $\omega_($ is $\omega_0 - \omega_1$, associated with the Moon. In the table, for the Doodson numbers, $\omega = \omega_($ and hence $\omega_\odot = \omega_(+ \omega_1 - \omega_2$. Note that the table also includes the K_2^S harmonic, even though it's amplitude is less than 0.05. Its frequency coincides with that of K_2^M and they are completely indistinguishable. They are combined into the single lunar-solar semi-diurnal wave, K_2. *From Bartels* [2].

Lecture 2: The Role of Tidal Dissipation and the Laplace Tidal Equations

Myrl Hendershott

1 Introduction

In this lecture we make a first attempt to describe the energetics of tides. We first provide some discussion of their influence on the global processes of the earth by relating tidally induced dissipation to the change in the earth's rotation rate, and consider whether there is any fossil evidence of such a change. We then approach this question of dissipation a little more formally, from the perspective of an angular momentum budget of the earth-moon system. Finally, we develop the dynamics of tides from first principles, starting with the Navier-Stokes equations on a rotating planet and finally obtaining the Laplace tidal equations.

2 Energetic Dissipation

We shall first consider the relationship between tidal dissipation and the rotation rate of the earth. If we neglect the internal dynamics of the earth, regarding it as a collection of processes that will eventually lead to dissipation, then the persistent energy of the planet is due to rigid-body rotation, whose rate of change is

$$E_t = \frac{\partial}{\partial t}\left(\tfrac{1}{2}C\Omega^2\right), \tag{1}$$

where C is the earth's moment of inertia along the polar axis and Ω is the earth's rotation rate. The change in Ω is then given by

$$\Omega_t = \frac{E_t}{C\Omega}. \tag{2}$$

Historically, astronomical data is used to infer Ω_t, which is then used to compute E_t. But to help motivate this relationship, we would like to compare it to some sort of observational record. For the moment, let us suppose that we have some rough estimate for the tidal dissipation. We may then use this to demonstrate how this lead to a variation in the length of day. Such variation could then leave an imprint in the fossil records, for example. So in

this case, if we use the following values,[1]

$$\begin{aligned} E_t &= -4.0 \times 10^{19} \text{ erg sec}^{-1}, \\ C &= 8.043 \times 10^{44} \text{ g cm}^2, \\ \Omega &= \frac{2\pi}{\text{the sidereal period}} = \frac{2\pi}{86164 \text{ sec}} \\ &= 7.292 \times 10^{-5} \text{ sec}^{-1}, \end{aligned}$$

then we would presume that the earth's rotation rate is currently decreasing at about

$$\Omega_t = -6.8 \times 10^{-22} \text{ rad sec}^{-2}.$$

We can use this to estimate the variation in length of day (LOD),[1]

$$\begin{aligned} \Delta(\text{LOD}) &= \tau' - \tau \\ &= 2\pi \left(\frac{1}{\Omega'} - \frac{1}{\Omega} \right), \end{aligned}$$

where

$$\Omega' = \Omega + \Delta\Omega \simeq \Omega + \Omega_t \Delta t,$$

so that

$$\begin{aligned} \Delta(\text{LOD}) &\simeq -\left(\frac{2\pi}{\Omega} \right) \left(\frac{\Omega_t}{\Omega} \right) \Delta t \\ &= 6.9 \times 10^{-8} \text{ sec} \end{aligned} \tag{3}$$

for $\Delta t = 1$ day $= 86400$ sec. Or, in more appropriate units,

$$\Delta(\text{LOD})/\text{day} = 2.5 \text{ msec cy}^{-1}.$$

As long as $\Omega_t \Delta t \ll \Omega$ remains a reasonably accurate statement, it should be possible to extrapolate about the LOD over epochal times. If we take $-\Delta t$ to be 400 million years, then $\Omega_t \Delta t \approx 0.12\Omega$ and our estimate for a constant LOD variation should be accurate within about 10%. Then in we compare the difference between current years and 400 million years ago, we find the following:

Today	365 days per year
400 Million Years Ago	414 days per year

Although mass factor has been neglected, this does demonstrate that there has likely been a significant change in both the dynamical and radiation cycle of the earth. A natural question is whether there is any evidence supporting the conjecture that the LOD was longer in the past, and how much Ω_t and E_t may have varied. The fossil record offers a possibility, since biological activity should be sensitive to rotation induced variations in the radiation cycle; this is explored in the next section.

[1]The angular rotation per day is slightly greater than 2π, but the error is insignificant for our purposes.

3 Biological Records

Several groups of organisms leave records in the skeletal parts of their accruing tissue, in the form of sequential and repetitive layers. These layers are interpreted in growth increments, and the sequence of layers appears to be a consequence of modulation of growth by internal rhythms inherent to the animal and environmental conditions.

Growth patterns that are controlled by astronomical phenomena are of particular interest. A comparison of frequencies found in living and fossil specimens may reveal indications of the constancy or periodicity of certain astronomical phenomena. One of the types of organisms that have been studied in a geophysical context is corals.

Seasonal fluctuations in the rate of coral growth were first reported by R. P. Whitefield in 1898, who described undulations on some surfaces of living corals and suggested that these represented annual growth increments associated with seasonal water temperature changes. However, the detailed mechanism by which growth occurs and the factors controlling the rate of growth are still inadequately understood.

The skeletal part of corals consist of several elements, one of which, the epitheca, reveals a fine structure of ridges that are parallel to the growing edge (figure 1). These ridges are interpreted as growth increments and they suggest a periodic fluctuation in the rate of calcium carbonate secretion. The rate of deposition of these growth increments in modern reef-forming corals is believed to be daily.

An indication that the growth ridges are daily is that modern corals typically add about 360 such increments per year, suggesting that the solar day controls the frequency of deposition[2, 3]. Although, factors other than variable daylight may be important here in modulating the growth rates, indirect evidence suggests that the solar day has remained the dominant periodicity in corals studied; Devonian corals studied by Wells[2] show about 400 daily growth increments between successive seasonal annulations, in keeping with expected value, if present tidal acceleration of the Earth has remained roughly constant over last $3\text{–}4 \times 10^8$ years. The same qualitative results can be found in molluscs and stromatolites too.

4 Angular Momentum

The consequences of tidal dissipation can also be seen in the receding of the moon from the earth. If we ignore the rotation of the moon and regard it as a point in space moving in a simple circular orbit, and again focus on the rigid-body rotation of the earth, then the total angular momentum of the earth-moon system is conserved and

$$\frac{\partial}{\partial t}\left(C\Omega + ml^2\omega\right) = 0, \tag{4}$$

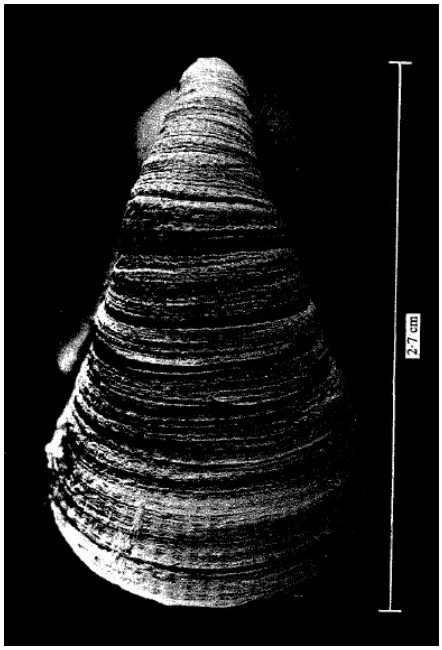

Figure 1: Middle Devonian coral epitheca from Michigan, U.S.A.

where m is the moon's mass, l is the orbital radius, and ω is the orbital frequency. These parameters currently have values of

$$\begin{aligned} m &= 7.35 \times 10^{25} \text{ g}, \\ l &= 3.84 \times 10^{10} \text{ cm}, \\ \omega &= \frac{2\pi}{27.32166 \times 86400 \text{ sec}} = 2.66 \times 10^{-6} \text{ rad sec}^{-1}. \end{aligned}$$

Expansion of the angular momentum equation gives

$$C\Omega_t + m\left(2l\omega l_t + l^2\omega_t\right) = 0.$$

To relate the change in distance to the change in frequency, we note that since the motion is assumed circular,

$$\frac{GMm}{l^2} = m\omega^2 l,$$

so that

$$\omega^2 l^3 = GM \quad \text{(Kepler's Third Law)},$$

and hence

$$\omega_t = -\frac{3}{2}\left(\frac{\omega}{l}\right) l_t. \tag{5}$$

We then obtain an expression for the rate at which the moon drifts from the earth,

$$l_t = -\frac{2C\Omega_t}{ml\omega}. \tag{6}$$

Laser ranging of the moon tells us that

$$l_t = 3.8 \text{ cm yr}^{-1} = 1.2 \times 10^{-7} \text{ cm sec}^{-1}$$

from which we infer that the change in the lunar cycle is

$$\omega_t = -1.25 \times 10^{-23} \text{ rad sec}^{-2} = -25.7'' \text{ cy}^{-2}.$$

This simple estimate is in close agreement with a more sophisticated calculation by Brosche and Sündermann, who obtained a result of $-26.06''$ cy^{-2}.[4]

From (6), we find that the rate of change of the earth's rotation is

$$\Omega_t = -5.6 \times 10^{-22} \text{ rad sec}^{-1}.$$

Based on this rotation rate, the loss of energy of the moon, from (2), is

$$E_t = -3.3 \times 10^{19} \text{ erg sec}^{-1} = -3.3 \text{ TW}$$

which, despite our idealizations, is in fairly good agreement with more sophisticated astronomical calculations of 3.75 ± 0.08 TW for lunar dissipation.[5]

5 Terrestrial Coordinates and the Traditional Approximation

In this section we consider the dynamics of a shallow fluid on a rotating planet. Later sections will introduce further approximations, which will lead us to the Laplace tidal equations (LTE) for each vertical mode.

The Navier-Stokes equations for an incompressible rotating fluid in spherical (terrestrial) coordinates are

$$\frac{D_s u}{Dt} - \left[2\Omega + \frac{u}{r\cos\theta}\right] v \sin\theta + \left[2\Omega + \frac{u}{r\cos\theta}\right] w\cos\theta = -\frac{p_\phi}{\rho r\cos\theta} - \frac{\Phi_\phi}{r\cos\theta} + X, \tag{7a}$$

$$\frac{D_s v}{Dt} + \left[2\Omega + \frac{u}{r\cos\theta}\right] u\sin\theta + \left[\frac{v}{r}\right] w = -\frac{p_\theta}{\rho r} - \frac{\Phi_\theta}{r} + Y, \tag{7b}$$

$$\frac{D_s w}{Dt} - \left[\frac{v}{r}\right] v - \left[2\Omega + \frac{u}{r\cos\theta}\right] u\cos\theta = -\frac{p_r}{\rho} - \Phi_r + Z, \tag{7c}$$

$$\frac{1}{r\cos\theta}\left[u_\phi + (v\cos\theta)_\theta\right] + \frac{1}{r^2}\left(r^2 w\right)_r = 0, \tag{7d}$$

where θ and ϕ are the latitude and longitude, Φ is the geopotential, and $\mathbf{X} = (X, Y, Z)$ represent dissipative forces. The advective derivative, $\frac{D_s}{Dt}$, is

$$\frac{D_s}{Dt} = \frac{\partial}{\partial t} + \frac{u}{r\cos\theta}\frac{\partial}{\partial\phi} + \frac{v}{r}\frac{\partial}{\partial\theta} + w\frac{\partial}{\partial r}$$

and the self-gravitating potential of the earth, including centrifugal forcing, is

$$\Phi = -\frac{GM_E}{r} + A(r,\theta) - \frac{1}{2}\Omega^2 r^2\cos^2\theta, \tag{8}$$

where $A(r,\theta)$ describes the deviation of gravitation from that of a spherical earth.

The centrifugal forcing of the earth causes the earth to deform, so that the equilibrium shape is closer to an oblate spheroid than a perfect sphere. But since the geopotentials are also deformed to match the shape of the earth, this tends to produce a situation that is only a slight distortion of the purely spherical dynamics. Veronis [6] has shown that the actual dynamics can be explicitly written as a perturbation series in terms of the ellipticity of the earth, e, with the leading order equations corresponding to dynamics on a sphere of radius $a = \frac{1}{2}(r_{\text{eq}} + r_{\text{pole}})$ and a uniform gravitational acceleration. The errors are more or less bounded by $\frac{3}{2}e \approx \frac{1}{200}$, or 0.5%, so it is generally reasonable to treat the earth as spherical if we restrict ourselves to large-scale flows.

The full set of equations satisfy the usual conservation laws. For example, if we neglect gravitational and dissipative forcing, the kinetic energy of a fluid parcel is balanced by the work due to pressure,

$$\frac{D_s}{Dt}\left[\frac{u^2+v^2+w^2}{2}\right] = -\frac{\mathbf{u}\cdot\nabla p}{\rho} \tag{9}$$

and the angular momentum is balanced by the pressure torque,

$$\frac{D_s}{Dt}\left[r\cos\theta\left(u+\Omega r\cos\theta\right)\right] = -\frac{p_\phi}{\rho}. \tag{10}$$

When integrated over the earth, both quantities are conserved.

From incompressibility $\left(\frac{W}{H} \ll \frac{U}{L}\right)$ and a shallow water aspect ratio ($H \ll L$), we expect a scaling where $W \ll U$ and that it is reasonable to neglect the centrifugal and Coriolis forces involving w and to replace r by a. But these changes also disrupt the conservation of energy and angular momentum unless we also neglect the centrifugal and Coriolis forces in z. This so-called *traditional approximation* is not always justifiable from scale analysis for flows of a homogeneous fluid shell , but it does produce a set of equations that is generally consistent with terrestrial fluid flow.

After applying the traditional approximation, we have

$$\frac{D_{sa}u}{Dt} - \left[2\Omega + \frac{u}{a\cos\theta}\right] v\sin\theta = -\frac{p_\phi}{\rho a\cos\theta} + X, \tag{11a}$$

$$\frac{D_{sa}v}{Dt} + \left[2\Omega + \frac{u}{a\cos\theta}\right] u\sin\theta = -\frac{p_\theta}{\rho a} + Y, \tag{11b}$$

$$\frac{D_{sa}w}{Dt} = -\frac{p_z}{\rho} - g + Z, \tag{11c}$$

$$\frac{1}{a\cos\theta}\left(u_\phi + (v\cos\theta)_\theta\right) + w_z = 0, \tag{11d}$$

where $z = r - a$ is the displacement from the earth's surface, D_{sa}/Dt is the advective derivative with $r = a$, and $g = GM_E/a^2$ is the radial acceleration due to the (now spherical) geopotentials.

6 Boussinesq Approximation

Because density variations are expected to be small, it is appropriate to introduce a Boussinesq approximation, where we only consider small variations from a hydrostatic basic state. Let p_0 denote the hydrostatic pressure, and also let $\overline{\rho}_0$ be the mean density and $\rho_0(z)$ the steady state variation from $\overline{\rho}_0$. Then since $\mathbf{u} = 0$ and $\mathbf{X} = 0$ at equilibrium, $p_0 = p_0(z)$ and

$$\frac{d\overline{p}}{dz} = -\left(\overline{\rho}_0 + \rho_0\right) g. \tag{12}$$

So if $p = p_0 + p'$ and $\rho = \overline{\rho}_0 + \rho_0 + \rho'$, then the hydrostatic balance is removed and, to leading order in density, the equations are

$$\frac{Du}{Dt} - \left[2\Omega + \frac{u}{a\cos\theta}\right] v \sin\theta = -\frac{p'_\phi}{\overline{\rho}_0 a\cos\theta} + X, \tag{13a}$$

$$\frac{Dv}{Dt} + \left[2\Omega + \frac{u}{a\cos\theta}\right] u \sin\theta = -\frac{p'_\theta}{\overline{\rho}_0 a} + Y, \tag{13b}$$

$$\frac{Dw}{Dt} = -\frac{p'_z}{\overline{\rho}_0} - g\frac{\rho'}{\overline{\rho}_0} + Z, \tag{13c}$$

$$\frac{1}{a\cos\theta}\left(u_\phi + (v\cos\theta)_\theta\right) + w_z = 0, \tag{13d}$$

$$\frac{D}{Dt}\left(\rho_0 + \rho'\right) = 0, \tag{13e}$$

where the thermodynamic incompressibility equation has been written explicitly, and the advective derivative subscript has been dropped.

Since the study of tidal dynamics focuses on the generation and propagation of gravitationally forced tidal waves, we will use the linearized Boussinesq equations. If we also assume that the perturbation flow is hydrostatic, then the system of equations for freely propagating waves is

$$u_t - (2\Omega\sin\theta)\, v = -\frac{p_\phi}{\overline{\rho}_0 a\cos\theta}, \tag{14a}$$

$$v_t + (2\Omega\sin\theta)\, u = -\frac{p_\theta}{\overline{\rho}_0 a}, \tag{14b}$$

$$0 = -\frac{p_z}{\overline{\rho}_0} - g\frac{\rho}{\overline{\rho}_0}, \tag{14c}$$

$$\frac{1}{a\cos\theta}\left(u_\phi + (v\cos\theta)_\theta\right) + w_z = 0, \tag{14d}$$

$$\rho_t = \frac{\overline{\rho}_0}{g} N^2 w, \tag{14e}$$

where the buoyancy frequency is

$$N(z) = \left(-\frac{g}{\overline{\rho}_0}\frac{d\rho_0}{dz}\right)^{\frac{1}{2}}$$

and primes have been dropped. The vertical velocity w becomes a diagnostic variable that can be computed from the density (thermodynamic) equation.

The original system was assumed to be incompressible. If we had included compressible effects, then the only major difference under the Boussinesq approximation would be that the buoyancy frequency is

$$N(z) = \left(-\frac{g}{\overline{\rho}_0} \frac{d\rho_0}{dz} - \frac{g^2}{c^2} \right)^{\frac{1}{2}},$$

where c is the speed of sound.

7 Vertical Mode Decomposition

Under certain situations, such as in the absence of a mean flow and with flat topography, we can decompose our solutions into a set of *vertical modes*, where each mode corresponds to the flow of a shallow water fluid. This provides an interpretation that relates the stratified continuum to a sequence of layered fluids, and isolates the barotropic waves (the unstratified dynamics) from the baroclinic waves. The analysis here closely follows Pedlosky.[7]

For a flat bottom (at, say, $z = -D_*$) we can separate the variables of the problem into a function of z and a function of horizontal and time variables so that

$$\begin{aligned} u &= U(\phi, \theta, t)F(z), \\ v &= V(\phi, \theta, t)F(z), \\ w &= W(\phi, \theta, t)G(z), \\ p &= \overline{\rho}_0 g \zeta(\phi, \theta, t)F(z). \end{aligned}$$

When we insert these expressions into the equations of motion, the horizontal momentum equations become

$$\begin{aligned} U_t - fV &= -\frac{g\zeta_\phi}{a\cos\theta}, \\ V_t + fU &= -\frac{g\zeta_\theta}{a}. \end{aligned}$$

Now let us apply these forms to the continuity equation,

$$\frac{U_\phi}{a\cos\theta} + \frac{(V\cos\theta)_\theta}{a\cos\theta} = -W\frac{G_z}{F}.$$

All terms except the ratio $\left(\frac{G_z}{F}\right)$ are independent of z while each term of this ratio is a function only of z. The only way this can hold for every z is if both sides equal a constant. Let us define this constant as

$$\frac{G_z}{F} \equiv \frac{1}{h}.$$

Then the continuity equation becomes

$$\frac{U_\phi}{a\cos\theta} + \frac{(V\cos\theta)_\theta}{a\cos\theta} + \frac{W}{h} = 0.$$

Applying the separable forms to the adiabatic equation yields

$$\zeta_t + W\frac{G}{F_z}\frac{N^2}{g} = 0,$$

which becomes

$$\zeta_t + W\frac{G}{G_{zz}}\frac{N^2}{gh} = 0.$$

Again we see that because ζ and W are not functions of z the coefficient of W must be constant. We can choose this constant to be -1 without any loss of generality (a different constant will only change the definition of h). With this choice the adiabatic equation becomes

$$\zeta_t = W.$$

This choice yields an equation for G,

$$G_{zz} + \frac{N^2}{gh}G = 0.$$

This is a homogeneous differential equation with, generally, non-constant coefficients since N is a function of z and there is a free parameter h. The problem is not complete until the boundary conditions are established. In order to have w vanish on $z = -D_*$ we must take

$$G(z) = 0, \quad z = -D_*.$$

At the free surface with a shallow water assumption the conditions are that the free surface displacement, which here we will call z_T satisfies

$$w = WG(z_T) = \frac{\partial z_T}{\partial t}.$$

While the total pressure is atmospheric pressure, which we will take to be a constant (zero), thus

$$P_{\text{total}} = p_0(z_T) + g\zeta F(z_T) = p_0(0) + \frac{dp_0}{dz}z_T + \ldots + \rho_0 g\zeta F(0).$$

Now keeping only linear terms let us derive the former equation with respect to time and combine it with the linearized kinematic equation,

$$\begin{aligned} 0 &= \frac{dp_0}{dz}\frac{\partial z_T}{\partial t} + \rho_0 g\zeta_t F(0), \\ 0 &= -\rho_0 gWG(0) + \rho_0 g\zeta_t F(0), \\ \rho_0 gWG(0) &= \rho_0 g\zeta_t F(0). \end{aligned}$$

But, from the continuity equation we know that,

$$\zeta_t = W,$$

thus,

$$G(0) = F(0) = hG_z(0).$$

Which means that the final condition for G is,

$$G_z - G/h = 0, \quad z = 0.$$

Let us summarize the equations for the resulting eigenvalue problem,

$$\begin{aligned} G_{zz} + \tfrac{N^2}{gh} G &= 0, \\ G &= 0, \qquad z = -D_*, \\ G_z - G/h &= 0, \qquad z = 0. \end{aligned}$$

Using the relations between F and G we obtain as an equally valid alternative problem,

$$\begin{aligned} \left(\tfrac{F_z}{N^2}\right)_z + \tfrac{1}{gh} F &= 0, \\ F_z &= 0, \qquad z = -D_*, \\ F_z - \tfrac{N^2}{g} F &= 0, \qquad z = 0. \end{aligned}$$

The advantage of the second formulation is that the eigenvalue h is not in the boundary condition. These equations can either be solved numerical for a varying N or examined analytically for the case of a constant N.

7.1 Vertical Modes For Constant N

Let us derive h for the case of a constant N. In this case the solution for $G(z)$, which satisfies the boundary condition at $z = -D_*$ is

$$G = A \sin m(z + D_*), \quad m^2 \equiv \tfrac{N^2}{gh},$$

where m is the vertical wavenumber of the solution. The eigenvalue relation for h is obtained from the boundary condition at $z = 0$, and yields,

$$m \cos(md) - \frac{1}{h} \sin(md) = 0,$$

or,

$$\tan(md) = mh = \frac{N^2}{gm},$$

or,

$$\tan(md) = \frac{N^2 d}{g} \frac{1}{md}.$$

We note that

$$\frac{N^2 d}{g} = -\frac{d\frac{d\rho_0}{dz}}{\rho_0} \simeq \frac{\Delta\rho_0}{\rho_0} \ll 1.$$

Thus, the roots of the dispersion relation split into two classes. The first class has roots for which md is order $O(1)$. In that case the right hand side of the dispersion relation is essentially zero and the solutions correspond to the zeros of the tangent function,

$$md = j\pi, \quad j = 1, 2, 3, \ldots.$$

In this approximation, there is an infinite number of roots corresponding to

$$m = -\frac{j\pi}{d}.$$

Therefore, from the definition of m we get,

$$h_j = -\frac{N^2 d^2}{g j^2 \pi^2}.$$

From this we can easily see that the modal structures are,

$$\begin{aligned} G_j &= \sin \tfrac{j\pi z}{d}, \quad j = 1, 2, 3, \ldots, \\ F_j &= \cos \tfrac{j\pi z}{d}, \quad j = 1, 2, 3, \ldots. \end{aligned}$$

Now let us consider the second class for which md is not of order $O(1)$ but, rather, $md \to 0$. Then, the dispersion relation becomes,

$$\tan(md) \simeq md = \frac{N^2 d}{g} \frac{1}{md}.$$

Therefore, from the definition of m we get,

$$h_0 = d,$$

which gives us the barotropic mode of zero vertical velocity with $m_0 \ll 1$ due to the almost no variation of F_0 in depth.

7.2 Vertical Modes For Slowly Varying N

Instead of assuming that stratification remains constant, a more realistic assumption would be to assume that N is slowly varying in some sense, for example if $dN/dz \ll N/l$ for some length scale l, such as the characteristic mode depth. If this remains true, then we can find an asymptotic solution using WKB methods.

If we rescale our equation in terms of a slow variable $Z = \epsilon z$, then the field equation for G is

$$\epsilon^2 G_{ZZ} + \frac{[N(Z/\epsilon)]^2}{g D_n} G = 0. \tag{15}$$

Since N is approximately constant, we have a WKB solution of the form

$$G \sim \exp\left[\frac{1}{\epsilon} S_0(Z) + S_1(Z)\right].$$

After substitution into the differential equation and matching powers of ϵ, we find that

$$S_0(Z) = \pm \frac{i}{\sqrt{g D_n}} \int_{-\epsilon D_*}^{Z} N(Z'/\epsilon) dZ', \tag{16a}$$

$$S_1(Z) = -\frac{1}{2} \ln\left[N(Z/\epsilon)\right], \tag{16b}$$

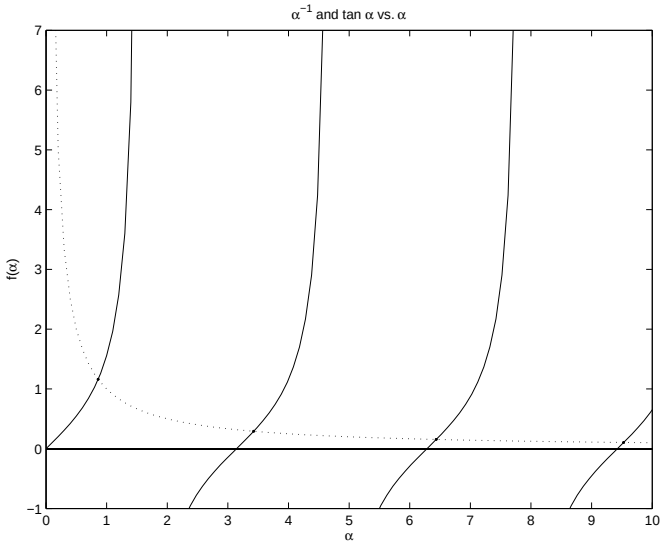

Figure 2: The solid line is the curve for $\tan\alpha$ and the dotted line is for α^{-1}. The intersection of the curves correspond to the roots of the equation $\alpha^{-1} = \tan\alpha$. As α increases, we see that the roots approach $\alpha = \pi n$.

so that G, in terms of z, becomes

$$G(z) \simeq \frac{1}{\sqrt{N(z)}} \exp\left[\pm \frac{i}{\sqrt{gD_n}} \int_{-D_*}^{z} N(z')dz'\right],$$

where by $\pm$, we mean that G is some linear combination of each solution.

We must now apply the boundary conditions to obtain a complete solution. From the surface condition, $G(z) = 0$ at $z = -D_*$, we see that

$$G(z) \simeq \frac{1}{\sqrt{N(z)}} \sin\left[\frac{1}{\sqrt{gD_n}} \int_{-D_*}^{z} N(z')dz'\right]. \tag{17}$$

From the upper condition, $G_z - G/D_n = 0$ at $z = 0$, and using the fact that dN/dz is small, we find that

$$N\sqrt{\frac{D_n}{g}} = \tan\left[\frac{1}{\sqrt{gD_n}} \int_{-D_*}^{0} N(z')dz'\right]. \tag{18}$$

If we let $\alpha_n = \sqrt{\frac{g}{N^2 D_n}}$, then solving for D_n is equivalent to solving for α_n in the equation

$$\frac{1}{\alpha_n} = \tan\left(k\alpha_n\right), \tag{19}$$

where $k = \frac{N}{g}\int_{-D_*}^{0} N(z')dz'$. The solutions to this equation for $k = 1$ are illustrated in figure 2. We can see that the roots correspond to $\alpha_n = \pi n/k$ as n becomes large so that

$$D_n \simeq \frac{\left[\int_{-D_*}^{0} N(z')dz'\right]^2}{g\pi^2 n^2}. \tag{20}$$

Although this is only formally correct for large n, the error is often small even for $n = 1$, and the accuracy only improves with increasing n, so that the WKB solution can usually be safely applied to the entire baroclinic spectrum.

8 Laplace Tidal Equations

From the above equations and the modal solution with respect to the z axis we can derive the Laplace tidal equations,

$$U_t - fV = -\frac{g\zeta_\phi}{a\cos\theta}, \tag{21a}$$

$$V_t + fU = -\frac{g\zeta_\theta}{a}, \tag{21b}$$

$$\frac{U_\phi}{a\cos\theta} + \frac{(V\cos\theta)_\theta}{a\cos\theta} + \frac{W}{h_j} = 0, \tag{21c}$$

$$\zeta_t = W. \tag{21d}$$

And if the two last equations are combined,

$$U_t - fV = -\frac{g\zeta_\phi}{a\cos\theta}, \tag{22a}$$

$$V_t + fU = -\frac{g\zeta_\theta}{a}, \tag{22b}$$

$$\zeta_t + h_j\left(\frac{U_\phi}{a\cos\theta} + \frac{(V\cos\theta)_\theta}{a\cos\theta}\right) = 0. \tag{22c}$$

This set of equations for each mode was considered for a flat bottom and with no external forcing. The friction and the tidal gravitational potential (TGP) can be introduced by simply decomposing these functions into their vertical modes. But since the TGP does not vary significantly across the shallow depth of the fluid, only the barotropic mode is excited noticeably when the bottom is flat, despite the fact that actual observations show strong baroclinic tides.

Although we will not discuss how to approach the full baroclinic case, we can consider the barotropic mode over a variable topography with a weakly elastic bottom (due to the elasticity of the earth). In this case, let $D(\theta, \phi)$ describe the mean depth of a homogeneous fluid, and δ denote the displacement of the elastic bottom. Then the equations for the barotropic mode are generalized to

$$u_t - (2\Omega\sin\theta)\, v = -\frac{g\,(\zeta - \Gamma/g)_\phi}{a\cos\theta} + \frac{F^\phi}{\rho D}, \tag{23a}$$

$$v_t + (2\Omega\sin\theta)\, u = -\frac{g\,(\zeta - \Gamma/g)_\theta}{a} + \frac{F^\theta}{\rho D}, \tag{23b}$$

$$(\zeta_t - \delta_t) + \frac{1}{a\cos\theta}\left[(uD)_\phi + (vD\cos\theta)\right] = 0, \tag{23c}$$

where Γ is the total tide generating potential. We will refer to these as the LTE. Note that an equation for the dynamics of the elastic bottom must be included to fully describe the system.

Notes by Yaron Toledo and Marshall Ward.

References

[1] K. Lambeck, *The Earth's Variable Rotation* (Cambridge University Press, Cambridge, 1980).

[2] J. W. Wells, "Coral growth and geochronometry," Nature **197**, 448 (1963).

[3] D. J. Barnes, "The structure and formation of growth-ridges in scleractinian coral skeletons," Proc. Roy. Soc. London **13**, 1 (1973).

[4] P. Brosche and J. Sündermann, in *Scientific Applications of Lunar Laser Ranging*, edited by J. D. Mullholland (D. Reidel, Dordrecht, 1977), pp. 133–141.

[5] L. H. Kantha, "Tides—a modern perspective," Marine Geodesy **21**, 275 (1998).

[6] G. Veronis, "Large scale ocean circulation," Advances in Applied Mathematics **13**, 1 (1973).

[7] J. Pedlosky, *Waves in the Ocean and Atmosphere: Introduction to Wave Dynamics* (Springer-Verlag, New York, 2003).

Lecture 3: Solutions to Laplace's Tidal Equations

Myrl Hendershott

1 Introduction

In this lecture we discuss assumptions involved in obtaining Laplace's Tidal Equations (LTE) from Euler's equations. We first derive an expression for the solid Earth tides. Solutions of LTE for various boundary conditions are discussed, and an energy equation for tides is presented.

Solutions to the Laplace Tidal equations for a stratified ocean are discussed in §2. We obtain expression for solid earth tide in §3. Different models of dissipation are examined in §4. Boundary conditions for LTE's are discussed in §5. In §6 the energy equation for LTE's is derived.

2 The Laplace Tidal equations for a Stratified ocean

To obtain the LTE for stratified ocean we assume pressure is hydrostatic and seek seperable solutions of the form

$$\begin{aligned} u(x,y,z,t) &= U(x,y,t)F_u(z), \\ w(x,y,z,t) &= W(x,y,t)F_w(z), \\ p(x,y,z,t) &= Z(x,y,t)F_p(z). \end{aligned}$$

The LTE for stratified ocean are

$$U_t - fV = -gZ_x \quad , \tag{1}$$

$$V_t - fU = -gZ_y \quad , \tag{2}$$

$$Z_t + D_n(U_x + V_y) = 0 \quad , \tag{3}$$

$$F_{w_{zz}} + \frac{N^2}{gD_n}F_w = 0 \quad , \tag{4}$$

where n is an index for the normal modes in the ocean. These equations are the constant depth LTE but where D_n is the equivalent depth of each mode, and $D_n \neq D_*$, rather

$$D_n = \frac{[\int_{-D_*}^{0} N(z')dz']^2}{gn^2\pi^2}$$

and $N(z)$ is the buoyancy frequency. For the zeroth mode or $n = 0, D_* \approx D$. The eigenvalue problem in (4) can be solved to determine the D_n using the following boundary conditions

$$\begin{aligned} F_w = 0 \quad &\text{at} \quad Z = -D_*, \\ F_w - D_n F_{w_z} = 0 \quad &\text{at} \quad Z = 0. \end{aligned}$$

2.1 Barotropic Solution (n = 0)

The normal mode equations described above and indexed by n an integer can be solved for specific modes. The zeroth order mode is given by $n = 0$ and is also called the barotropic or external mode. It is characterized by a solution which is depth independent. Below we will solve for the barotropic mode without rotation and no variations in the y direction ($f = 0$ and $\partial/\partial y = 0$). If we assume a plane wave solution, solving (1) - (4) gives,

$$\begin{aligned} Z_0 &= a e^{-i\sigma t + ikx} \ , \\ U_0 &= a \left(\frac{gk}{\sigma} \right) e^{-i\sigma t + ikx} \ , \\ \sigma &= \pm k \sqrt{g D_*}. \end{aligned}$$

Figure 1 shows the barotropic solution for velocity. For the semidiurnal tidal frequency, the phase velocity of the zeroth mode wave, given by $c_0 = \sqrt{gD_0} = \sigma/\kappa = 200$ m/s. Since this speed is also given by λ/T, where λ is the horizontal wavelength of the wave (distance from wave crest to wave crest), then $\lambda = 8640$ km. This wave is very fast and very long. For the case of no rotation this wave is dispersionless, but not when $f \neq 0$.

2.2 Baroclinic Solution, Mode 1 (n = 1)

The first baroclinic mode, indexed by $n = 1$ is also called the first internal mode. The rest of the modes for $n > 1$ are also internal modes and have more variation in depth. We can solve (1) - (4) for $n = 1$ without rotation and with no variations in y ($f = 0$ and $\partial/\partial y = 0$) giving the first internal mode,

$$\begin{aligned} Z_n &= a e^{-i\sigma t + ikx} \ , \\ F_{U_1} &= cos(\frac{\pi(z + D_*)}{D_*}) \ , \\ F_{W_1} &= sin(\frac{\pi(z + D_*)}{D_*}) \ , \\ \sigma &= \pm k \sqrt{g D_1}. \end{aligned}$$

The mode one solution is shown in figure 1. For the baroclinic modes, the phase velocity and horizontal wavelength are given by

$$\begin{aligned} c_n = \frac{N_0 D_*}{n\pi} = \frac{(1.45 \times 10^{-3})(4000m)}{n\pi} = \frac{1.85 \text{ m/s}}{n}, \\ \lambda_{tidal} = \frac{80 \text{ km}}{n}. \end{aligned}$$

So the lower modes travel more quickly, and have larger horizontal scales. The M_2 internal tide is found primarily as a mode 1 tide throughout the world's oceans, while higher order modes tend to dissipate nearer their source. Due to recent (last decade) improvements, the M_2 internal tide can now be seen by satellite altimetry. The ocean surface displacement due to internal tides is given by

$$\frac{w_{\text{free surface}}}{w_{\text{interior maximum}}} \approx \frac{N_0^2 D_*}{gn\pi} \approx 3 \times 10^{-4},$$

which means that for an internal tide displacement of isopycnals on the order of 100m (which is quite large but not impossible), the surface expression would be about 30cm, easily resolved by satellite altimetry measurements which have accuracy on the order of a few centimeters.

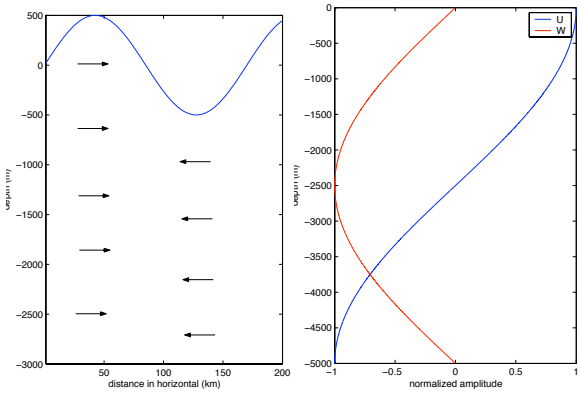

Figure 1: (a) Barotropic or depth independent solution for u velocity. Wave amplitude is greatly exaggerated. (b) Mode 1 solution for u and w velocity.

2.3 Numerical Solution to LTE

The complete problem that we would like to solve numerically to estimate the tides are the stratified linear equations,

$$u_t - fv = -\frac{p_x}{\rho_0} + \Gamma_x, \tag{5}$$

$$v_t + fu = -\frac{p_y}{\rho_0} + \Gamma_y, \tag{6}$$

$$\zeta_t + (uD)_x + (vD)_y = 0, \tag{7}$$

where Γ is full tide generating potential and $D(x, y)$ is the bottom topography. The domain is defined by the coasts of continents, ocean bottom and free surface. However, in order to solve this system of equations one must resolve short horizontal scales due to bottom topography where the bottom boundary condition on w is $w = -\mathbf{u} \cdot \nabla D$. Very few current modes are capable of this, though some have begun to resolve mode 1 in their simulations.

Instead the Laplace tidal equations for u and v may be substituted, of (5)-(7).

$$u_t - fv = -g\zeta_x + \Gamma_x, \tag{8}$$
$$v_t + fu = -g\zeta_y + \Gamma_y, \tag{9}$$

where ζ is the free surface and a smoother bottom topography is substituted,

$$w = -\mathbf{u} \cdot \nabla D_{smooth}. \tag{10}$$

However, because ζ is no longer a function of z while p in (5)-(7) was, we cannot determine $u(z)$ and (8)-(9) will only give the barotropic solution.

In the literature, the TGP is usually neglected and instead the barotropic tides and stratification are specified, which allows the simplification of (5)-(7) as

$$u_t - fv = -\frac{p_x}{\rho_0}, \tag{11}$$
$$v_t + fu = -\frac{p_y}{\rho_0}. \tag{12}$$

From this, the internal tides result from a single scattering of the barotropic tide by bottom relief $w_{int} = u_B \cdot \nabla D(x, y)$. In particular, if we decomposed D into low- and high-passed components,

$$D(x, y) = D_{lo}(x, y) + D_{hi}(x, y). \tag{13}$$

Then the ζ equation and bottom boundary conditions become

$$\zeta_{0t} + \nabla \cdot (\mathbf{u}_B D_{lo}(x, y)) = 0,$$
$$w_{int} = \mathbf{u}_B \cdot \nabla D_{hi}(x, y).$$

And the internal tide results from the bottom topography. However, this neglects multiple scattering from the topography and does not apply when the bottom slope is greater than the characteristic slope of internal waves. Currently, numerical models like the Princeton Ocean Model (POM) solve the (5)-(7). An example of numerically solved tides is shown in figure 2. In this paper, all tidal constituents were solved for using a hydrodynamic model and data assimilation from tide gauges and altimetry [1].

3 Solid Earth Tide

It has long been known that Earth's crust yields elastically to the tidal forces of the moon and sun. If we consider earth to be an incompressible elastic solid, then we can write equations for the deformation of the Earth as the following

$$-p_x + \mu\nabla^2 u = 0, \tag{14}$$
$$-p_z + \mu\nabla^2 w = 0. \tag{15}$$

where, p is pressure, (u, v) are the velocity and μ is viscosity of earth (see figure 3). Using the following boundary conditions,

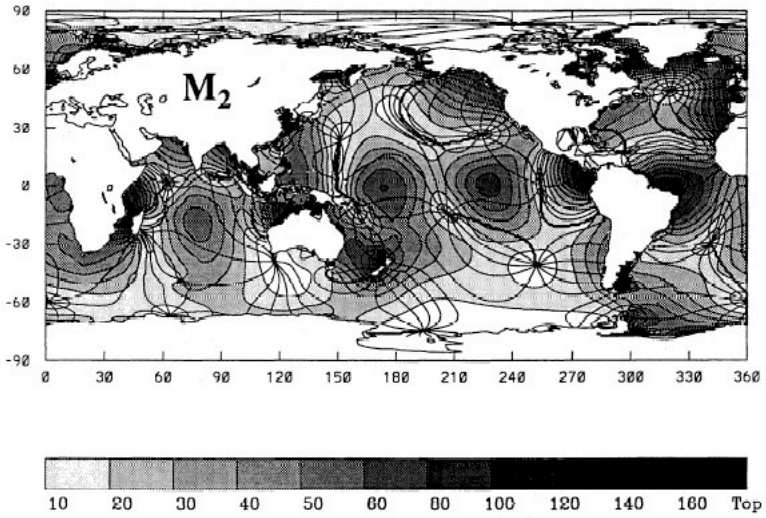

Figure 2: Cotidal map of the M_2 component. Coamplitude lines are drawn following the scaling indicated below the map. Units are in centimeters. Cophase lines are drawn with an interval of 30°, with the 0° phase as a larger drawing, referred to the passage of the astronomical forcing at Greenwich meridian [1].

$$u, w \to 0 \ as \ z \to -\infty,$$
$$\tau_{xz} = 2\mu(u_z + w_x) = 0 \ at \ z = 0,$$
$$\tau_{zz} = -p + 2\mu w_z = -\text{load} \ \equiv -\rho_w g a e^{ikx},$$

where term $\rho_w g a e^{ikx}$ gives the loading on earth surface due to ocean tide, a is the tidal amplitude and k is its horizontal wavenumber, we solve (14) and (15) with the above b.c.'s for a load of $\rho_w g a e^{ikx}$ to get an Earth surface wave displacement of

$$h\rho_w g a e^{ikx}, \tag{16}$$

where h is called "Love Number". In this case, $h = \frac{1}{2\mu k}$.

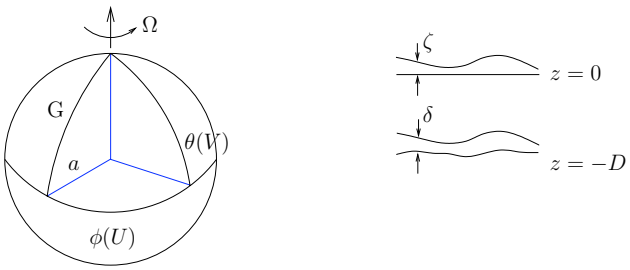

Figure 3: Solid earth tide, ζ is geocentric surface tide and δ is geocentric solid earth tide.

We can then write the tide generating potential in spherical harmonic (n) decomposition including the solid Earth tide as,

$$\Gamma_n = U_n + k_n U_n + q\alpha_n \zeta_{on} + k'_n q\alpha_n \zeta_{on}, \tag{17}$$

where U_n is obtained from astronomy, $k_n U_n$ is earth yielding to astronomical potential, $q\alpha_n\zeta_{on}$ is potential of tidal shell and $k'_n q\alpha_n\zeta_{on}$ is earth yielding to tidal potential.

Proceeding as above, solid earth tide is given as,

$$\delta_n = h_n \frac{U_n}{g} + h'_n \alpha_n \zeta_{on}. \tag{18}$$

k_n, k'_n, h_n and h'_n are all "Love numbers" similar to h in (16). From (17) and (18) we find

$$\left(\frac{\Gamma}{g} - \delta\right)_n = \left(\frac{1 + k_n - h_n}{g}\right) U_n + (1 + k'_n - h'_n)\alpha_n \zeta_{on}. \tag{19}$$

And upon summing up this series we get Farrell Green's function [2]

$$\sum_n (1 + k'_n - h'_n)\alpha_n \zeta_{on} = \int\int d\theta' d\phi' G_F(\theta', \phi' | \theta, \phi)\zeta_0(\theta', \phi'). \tag{20}$$

Now taking into account the solid Earth tide, we can rewrite Euler's equations from Lecture 2 as

$$\zeta_0 = \zeta - \delta \ , \tag{21}$$

$$u_t - (2\Omega\, sin\theta)v = -\frac{g(\zeta_0 - (\Gamma/g - \delta))_\phi}{a\, cos\theta} + \frac{F^\phi}{\rho D} \ , \tag{22}$$

$$v_t + (2\Omega\, sin\theta)u = -\frac{g(\zeta_0 - (\Gamma/g - \delta))_\theta}{a} + \frac{F^\theta}{\rho D} \ , \tag{23}$$

$$\begin{aligned}(\zeta_{ot} - \delta_t) + \frac{1}{a\, cos\theta}[(uD)_\phi + (vD\, cos\theta)_\theta] = &-\sum_n \left(\frac{1 + k_n - h_n}{g}\right) U_n \\ &- \int\int d\theta' d\phi' G_F(\theta', \phi' | \theta, \phi)\zeta_0(\theta', \phi') \ ,\end{aligned} \tag{24}$$

where U is mostly U_2, $k_2 \approx 0.29$ and $h_2 \approx 0.59$.

4 Dissipation Models

It is not easy to estimate the dissipation terms (F^θ and F^ϕ) in (22) and (23). This dissipation is mainly due to bottom drag and internal tides. If we model it as bottom drag, we get

$$\underline{F} = -\rho C_D |\underline{u}| \underline{u}, \tag{25}$$

where $C_D \approx 0.0025$ known from direct measurement in shallow water. The direct effect of (25) is that most of dissipation is limited to shallow seas where u and C_D are large. However, global tidal computations are mostly confined to deep-water zones for practical reasons (shallow water tides require much finer grid-spacing). So dissipation can only be properly represented by radiation of energy out of the model into bounding seas.

There are two main empirical models used to get an expression for dissipation in deep oceans. These are,

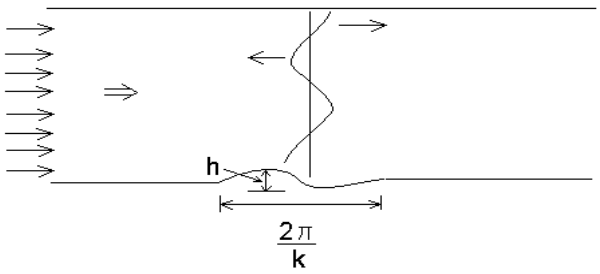

Figure 4: Jayne & Laurent model, dissipation due to barotropic tide scattering into internal tides over rough topography.

Jayne & Laurent In their runs of the Hallberg Isopycnal Model (HIM), the dissipation term is modeled as,

$$\underline{F} = -\frac{1}{2}\rho k h^2 N_b \underline{u}. \tag{26}$$

This model is based on assumption that dissipation occurs due to barotropic tide scattering into internal tides due to the rough bottom topography. h represents the height of bottom topography whose dominant horizontal wavenumber is k (see figure 4).

Arbic In his runs of the HIM for the dissipation term we have,

$$\begin{aligned} \underline{F} &= -p'_{IW} \nabla h \\ &= \rho(\nabla\chi \cdot \underline{u})\underline{\nabla} h, \end{aligned} \tag{27}$$

where,

$$\chi = \frac{N_b\sqrt{\sigma^2 - f^2}}{2\pi\sigma} \int\int \frac{h(x')}{|x - x'|} dx'dy' \tag{28}$$

for tide of frequency σ. N_b is buoyancy freqency, f is the Coriolis parameter and $h(x)$ is bottom topography. Arbic's model is based on the assumption that tidal dissipation can be calculated by finding the pressure drop in tidal currents across topographic features at the bottom.

5 Boundary Conditions

Laplace tidal equations have never been solved well enough so as to remove tides from altimetry without data assimilation. Different methods use different boundary conditions for solution of LTE at numerical coast. Some of the main boundary conditions in use are,

1. $\underline{u} \cdot \hat{h} = 0$ at the numerical coast.
   This is the most commonly used boundary condition. This boundary condition represents a no-energy-flux coast. It is important to have correct information regarding dissipation if this boundary is used since all energy must be dissipated within the system. Numerical schemes need to resolve $-\rho C_D \underline{u}|\underline{u}|$ well which requires high resolution in shallow waters.

2. $\zeta = \zeta_{obs}$ at the numerical coast.
   This boundary condition allows a energy flux ($\rho g D|\underline{u}| \cdot \hat{h}\zeta$) through the coast. The scheme is less sensitive to the details of the dissipation model used, and is less sensitive to the discretization used. However, this system can still respond resonantly. Another problem with this scheme is that observed tidal data is not easily available along all coasts.

3. $\zeta = c\ (\underline{u} \cdot \hat{h})$ at the numerical coast.
   This boundary allows energy to be dissipated at coast. In this boundary the parameter c can be adjusted so as to get results to match the observed tidal results. This leads to an energy flux of $< \rho g D c \zeta^2 >$ flowing out of the coast.

6 Energetics

If we ignore the solid Earth tide, we can derive equations of energy and perhaps estimate dissipation due to the tides as a residual. Starting with Laplace's tidal equations,

$$\begin{aligned} u_t - fv &= -g(\zeta - \Gamma/g)_x + F^x/\rho D \qquad \times \rho u D \\ v_t + fu &= -g(\zeta - \Gamma/g)_y + F^y/\rho D \qquad \times \rho v D \\ \zeta_t + (uD)_x + (vD)_y &= 0 \qquad \times \rho g \zeta \end{aligned}$$

Then multiplying by the terms at right, adding the three equations together and assuming that ρ, g and D are constant, we arrive at

$$\frac{1}{2}\rho D(u^2 + v^2)_t + \frac{1}{g}\rho g(\zeta^2)_t + \nabla \cdot (\rho g \zeta u D) = \rho \zeta_t \Gamma + \nabla \cdot (\rho u D \Gamma) + u \cdot F \tag{29}$$

$$KE_t + PE_t + \nabla \cdot Eflux = \begin{array}{c} \textit{Fluid crossing} \\ \textit{equipotentials} \\ \textit{vertically} \end{array} + \begin{array}{c} \textit{Fluid crossing} \\ \textit{equipotentials} \\ \textit{horizontally} \end{array} + \begin{array}{c} \textit{Work by} \\ \textit{dissipative} \\ \textit{forces} \end{array} \tag{30}$$

where KE_t is the time derivative of kinetic energy, PE_t is the time derivative of potential energy, and $Eflux$ is energy flux.

Energy Averaged Over One Tidal Period, Integrated Over the Ocean

It is convenient to consider the energy as averaged over one tidal period. For a periodic tide, let $< \cdot >$ denote the average over one period. This will simplify the above equations, since

$$< KE_t > = < PE_t > = 0. \tag{31}$$

Then from (29) we are left with

$$\nabla \cdot < P > = < W_t > + < u \cdot F >, \tag{32}$$

where P is energy flux and W_t is the working by potential vertical and horizontal forces.

Now if we reconsider the case of the basin with no flow through its boundaries ($\vec{u} \cdot < \hat{n} > = 0$), then we further have that $\int \nabla \cdot < P > dxdy = 0$ since there can be no

net energy flux into or out of the basin. Then we can integrate the remaining terms in the energy equation over the ocean basin and find that

$$\int < W_t > dxdy = \int_{ocean} \rho\zeta_t \Gamma dxdy = -\int_{ocean} < u \cdot F > dxdy. \tag{33}$$

One caveat is that the solid Earth tide is not dissipation free, i.e. the Love numbers are complex, but this equation is true provided that they are real. Now, since $-\int < u \cdot F > dxdy$ is balanced by working of fluid moving up and down. This fluid movement ζ can be measured from global altimetry, giving an estimate if dissipation of energy due to the tides.

6.1 Including the solid earth tide

If we now include the solid Earth tide, then our third equation becomes

$$(\zeta - \delta)_t + \nabla \cdot \vec{u} D = 0 \tag{34}$$

and if we follow the same procedure as before we have

$$\begin{aligned} KE_t &= -\nabla \cdot (\rho g D \vec{u}(\zeta - \Gamma/g)) + \rho g(\zeta - \Gamma/g)\nabla \cdot \vec{u} D + u \cdot F \\ &= -\nabla \cdot (\rho g D \vec{u}(\zeta - \Gamma/g)) - \rho g(\zeta - \Gamma/g)(\zeta_t - \delta_t) + \vec{u} \cdot F \\ &= \nabla \cdot \rho D u \Gamma + \rho(\zeta - \delta)_t \Gamma - \nabla \cdot \rho g D u \zeta - \rho g \zeta(\zeta - \delta)_t + u \cdot F. \end{aligned}$$

Similarly for potential energy,

$$\begin{aligned} PE &= \int_{-D+\delta}^{\zeta} \rho g z dz = \frac{1}{2}\rho g(\zeta^2 - (-D + \delta)^2), \\ PE_t &= \rho g(\delta\delta_t - \zeta\zeta_t - D\zeta_t). \end{aligned}$$

Adding these together we find that

$$\begin{aligned} KE_t + PE_t + \nabla \cdot (\rho g u D \zeta) &= \nabla \cdot \rho D u \Gamma + \rho(\zeta - \delta)_t \Gamma + u \cdot F \\ &\quad - \rho g \zeta(\zeta_t - \delta_t) + \rho g(\zeta\zeta_t - \delta\delta_t + D\delta_t) \\ &= \nabla \cdot \rho D u \Gamma + D u \Gamma + \rho(\zeta - \delta)_t \Gamma + u \cdot F + \rho g(\zeta - \delta + D)\delta_t. \end{aligned}$$

Then if we consider the observed tide only, $\zeta_0 = \zeta - \delta$, the difference between the ocean tides and the solid earth tide, we have the energy equation.

$$KE_t + PE_t + \nabla \cdot \vec{P} = W_t + u \cdot F, \tag{35}$$

with

$$KE = \frac{1}{2}\rho D(u^2 + v^2), \tag{36}$$

$$PE = \frac{1}{2}\rho g(\zeta_0^2 + 2\zeta_0\delta + 2\delta D), \tag{37}$$

$$\vec{P} = \rho g D \vec{u}(\zeta_0 + \delta), \tag{38}$$

$$W_t = \rho\zeta_{0_t}\Gamma + \rho\nabla \cdot u D \Gamma + \rho g(\zeta_0 + D)\delta_t. \tag{39}$$

Energy Averaged Over One Tidal Period, Integrated Over the Ocean

If we again average over one tidal period, then

$$\nabla\cdot < P >=< W_t > + < u \cdot F > \tag{40}$$

Given altimeter data ζ_1 it may be possible to map $< u \cdot F >$ [3].

If we further assume that the tides are periodic as $(e^{-i\sigma t})$, then noting that in the equation for W_t that $\int_{ocean} \rho\nabla \cdot uD\Gamma = 0$ and $< \rho g D\delta_t >= 0$,

$$\int_{oc} < W_t > dxdy = \frac{1}{2} Re \left\{ int_0 - \sigma\rho\zeta_0\Gamma^* + i\sigma g\rho\zeta_0\delta^* \right\},$$

where $(\cdot)^*$ is the complex conjugate. Using the Love number decomposition from §3,

$$\begin{aligned}\int_{oc} < W_t > dxdy &= \frac{1}{2} Re \int_0 \sum_n -i\sigma\rho\zeta_{0n} \left((1+k_n)u_n^* + g\alpha_n\zeta_{0n}^* + k_n' g\alpha_n\zeta_{0n}^* \right) \\ &\qquad + i\sigma\rho\zeta_{0n}(h_n u_n^* + \delta h_n'\alpha_n\zeta_{0n}^*) \\ &= \frac{1}{2} Re \sum_n \int -i\sigma\rho(1+k_n-h_n)\zeta_{0n}u_n^*. \end{aligned} \tag{41}$$

This last equation is true provided that the solid earth tide is dissipation-less, that is to say, that the Love numbers are real. Now, since again $\int_{ocean} \nabla\cdot < P > dxdy = 0$,

$$\int_{ocean} < u \cdot F > dxdy = \int_{ocean} < W_t > dxdy = \frac{1}{2} Re \sum_n \int -i\sigma\rho(1+k_n-h_n)\zeta_{0n}u_n^* \tag{42}$$

and we can estimate the dissipation of energy due to the tides if we know the observed tides, ζ_0.

Notes by Vineet Birman and Eleanor Williams Frajka

References

[1] C. L. Provost, M. L. Genco, F. Lyard, P. Vincent, and P. Canceil, "Spectroscopy of the world ocean tides from a finite element hydrodynamic model," J. Geophys. Res. **99**, 24777 (1994).

[2] W. E. Farrell, "The effect of ocean loading on tidal gravity," EME Symposium Marees Terrestres Strasbourg: OBS. ROY. BELG. COMM 116 .

[3] G. D. Egbert and R. D. Ray, "Significant dissipation of tidal energy in the deep ocean inferred from satellite altimeter data," Nature **405**, 775 (2000).

Investigator	Type of Model	Boundary Condition	Dissipation	Earth Tide
Zahel (1970)	M2, K1 tides for globe	Impermeable coast	Bottom stress in shallow water	None
Pekeris et al. (1969)	M2 tide for globe	Impermeable coast	Linearized artificial bottom stress in shallow water	None
Hendershott (1972)	M2 tide for globe	Coastal elevation specified	At coast only	None
Bogdanov et al. (1967)	M2, S2, K1, 01 tides for globe	Coastal elevation specified	At coast only	None
Tiron et al. (1967)	M2, S2, K1, 01 tides for plane model	Coastal elevation specified where data exist, otherwise impermeable coast	At coast only	None
Gohin (1971)	M2 tide for Atlantic, Indian Oceans	Coastal impedance specified	At coast only	Yielding to astronomical force only
Platzman (1972)	Normal modes for major basins, especially Atlantic	Adiabatic boundaries	Zero	-
Munk et al. (1970)	Normal mode representation of California coastal tides	Impermeable coast	Zero, although energy flux parallel to coast may reflect dissipation up coast	Yielding to astronomical force only
Cartwright (1971)	β plane representation for South Atlantic tides	Island values specified	Zero, although energy flux may reflect distant dissipation	Yielding to astronomical force only
Ueno (1964)	M2 tide for globe	Impermeable coast	None	None
Gordeev et al. (1972)	M2 tide for globe	Impermeable coast	Linearized bottom stress in shallow water	None

Table 1: Summary of Large-Scale Tidal Models.

Lecture 4: Resonance and Solutions to the LTE

Myrl Hendershott and Chris Garrett

1 Introduction

Myrl Hendershott concluded the last lecture by discussing the normal modes of the ocean, i.e. the free wave solutions of the Laplace Tidal equations. Today, we will review these concepts and extend them to so solve for specific instances of gravity and Rossby modes in simple basins. We will then discuss the computation work of Platzman [1] on the normal modes in the oceans and describe resonance in the seas.

The second half of the lecture was given by Chris Garrett and served as an introduction to his lectures during the second week. He motivates the study of tides by discussing them in the contexts of observations at several different geographical locations. He then adds to Myrl Hendershott's discussion on resonance with observations and some inferences about friction.

2 Review of Normal Modes

In plane coordinates, the Laplace Tidal equations (LTE) are given by

$$\begin{aligned} u_t - fv &= -g\zeta_x, && (1)\\ v_t + fu &= -g\zeta_y, && (2)\\ \zeta_t + D\left(u_x + v_y\right) &= 0, && (3) \end{aligned}$$

where $f = f_0 + \beta y$ and $D = D_n$, where D_n is a constant determined by an appropriate eigenvalue problem discussed in the previous lecture. To find free solutions of the LTE we look for harmonic solutions, i.e. solutions with time dependence proportional to $e^{-i\sigma t}$ which can be seen as transforming the time derivatives by

$$\frac{\partial}{\partial t} \rightarrow -i\sigma. \tag{4}$$

That is, the LTE become

$$\begin{aligned} -i\sigma u - fv &= -g\zeta_x, && (5)\\ -i\sigma v + fu &= -g\zeta_y, && (6)\\ -i\sigma\zeta + D\left(u_x + v_y\right) &= 0. && (7) \end{aligned}$$

Solving for u and ζ in terms of v, the LTE can be reduced into a single second order partial differential equation for v. We find that

$$\nabla^2 v + i\frac{\beta}{\sigma}v_x + \frac{\sigma^2 - f^2}{gD}v = 0. \tag{8}$$

If we seek plane wave solutions for v i.e. $v = e^{-i\sigma t + ikx + ily}$, then (8) implies that

$$-k^2 - l^2 - \frac{\beta k}{\sigma} + \frac{\sigma^2 - f_0^2}{gD} = 0. \tag{9}$$

This relation between k, l and σ is more useful when rewritten as

$$\left(k - \frac{\beta}{2\sigma}\right)^2 + l^2 = \left(\frac{\beta}{2\sigma}\right)^2 + \frac{\sigma^2 - f_0^2}{gD}. \tag{10}$$

We see from this equation that high and low frequency waves have significantly different character in the $k - l$ plane. High frequency waves, correspond to $\beta = 0$ which give circles centered at the origin with wavelength $\left(\left(\sigma^2 - f_0^2\right)/gD\right)^{1/2}$. These correspond to gravity modes which are characterized by $\sigma > f$ and are discussed in Section 3. For low frequencies, we have circles centered at $k = \beta/2\sigma$, $l = 0$ with radius less than $\beta/2\sigma$ so that the circles are entirely in the $k > 0$ plane. These are known as Rossby modes and are discussed in Section 4.

A third type of free wave is due to the influence of rotation. These "Kelvin" waves move along the direction of the physical boundary, e.g. the coast of a continent, and decay in magnitude as the distance from the boundary increases. For large enough basins, sum of the normal modes consist of an integral number of Kelvin waves around the boundary. An example of this will be seen in the discussion of gravity waves in a circular basin in Section 3.

3 Gravity Modes

It is instructive to solve the LTE in the context of some very simplified cases first, because the resulting motions are simplified illustrations of the true dynamics. If there is no rotation ($f = 0$), the LTE are given by

$$u_t = -g\zeta_x, \tag{11}$$

$$v_t = -g\zeta_y, \tag{12}$$

$$\zeta_t + D_0(u_x + v_y) = 0, \tag{13}$$

with the boundary condition that

$$\mathbf{u} \cdot \hat{\mathbf{n}} = 0 \tag{14}$$

at the coast, where $\hat{\mathbf{n}}$ is the unit vector normal to the coast. Substituting (11)-(12) into (13), we attain a Helmholtz equation:

$$\nabla^2 \zeta + (\sigma^2/gD)\zeta = 0, \tag{15}$$

with

$$\vec{\nabla}\zeta \cdot \hat{\mathbf{n}} = 0 \tag{16}$$

at the coast.

3.1 Square Basin

We first consider a rectangular basin (Fig. 1) with $A > B$. A general solution can be found by substituting

$$\zeta_{nm} = e^{-i\sigma_{nm}t} \cos\left(\frac{n\pi x}{A}\right) \cos\left(\frac{m\pi y}{B}\right) \tag{17}$$

into (15), which gives the dispersion relation

$$\sigma_{nm}^2 = gD_0 \left[\left(\frac{n\pi}{A}\right)^2 + \left(\frac{m\pi}{B}\right)^2\right]. \tag{18}$$

The gravest mode is then given by

$$T_{10} = \frac{2A}{\sqrt{gD_0}}, \tag{19}$$

where A is the length of the longer side. For all subsequent modes of oscillation,

$$T_{mn} > \frac{2A}{\sqrt{gD_0}}. \tag{20}$$

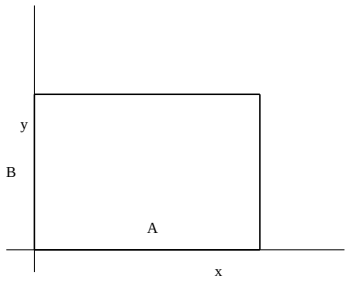

Figure 1: Rectangular ocean basin.

3.2 Circular Basin

In the real world, of course, ocean basins are not rectangular. The next general case that we can consider is that of a circular basin (figure 2). In this case, it is helpful to transform (15) to polar coordinates:

$$\zeta_{rr} + \frac{\zeta_r}{r} + \frac{\zeta_{\phi\phi}}{r^2} + \frac{\sigma^2}{gD_0}\zeta = 0, \tag{21}$$

with boundary condition

$$\zeta_r|_{r=a} = 0. \tag{22}$$

The general solution, which can be derived using separation of variables, is then given by

$$\zeta_{ns} = J_s(\kappa_{ns} r) e^{-i\sigma_{ns}t + is\phi}. \tag{23}$$

The appropriate eigenvalues for the κ_{ns} are determined by the boundary condition; that is

$$J_s'(\kappa_{ns}a) = 0. \tag{24}$$

Finally, the dispersion relation, obtained by plugging (23) into (21), is

$$\sigma_{ns}^2 = gD_0\kappa_{ns}^2. \tag{25}$$

This dispersion relation produces an ascending sequence of eigenfrequencies, σ_{ns}^2.

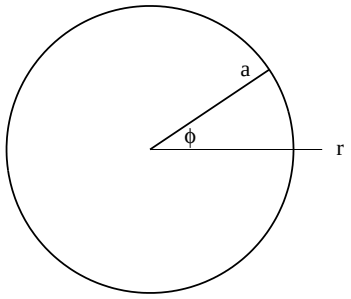

Figure 2: Circular ocean basin.

3.3 Circular Basin with Rotation

We can now add rotation to the problem in a simple way, but setting the Coriolis parameter $f = f_0$. For simplicity, we will keep the depth constant ($D = D_0$). The tidal equations are now given by

$$\begin{aligned} u_t - f_0 v &= -g\zeta_x, & (26)\\ v_t + f_0 u &= -g\zeta_y, & (27)\\ \zeta_t + D_0(u_x + v_y) &= 0, & (28) \end{aligned}$$

with the boundary condition, as before, given by (14). The Helmholtz equation can then be similarly derived, and is given by

$$\nabla^2\zeta + (\frac{\sigma^2 - f_0^2}{gD_0})\zeta = 0, \tag{29}$$

with the boundary condition

$$-i\sigma\zeta_n - f_0\zeta_s = 0 \tag{30}$$

at the coast.

Separable solutions now occur only in a circular basin. In polar coordinates, the Helmholtz equation with rotation is given by

$$\zeta_{rr} + \frac{\zeta_r}{r} + \frac{\zeta_{\phi\phi}}{r^2} + \frac{\sigma^2 - f_0^2}{gD_0}\zeta = 0, \tag{31}$$

with boundary condition

$$-i\sigma\zeta_r - \frac{f_0\zeta_\phi}{a} = 0. \tag{32}$$

The general solution is again given by (23), but now with a modified dispersion relation,

$$\sigma_{ns}^2 = f_0^2 + gD_0\kappa_{ns}^2. \tag{33}$$

For $s = 0$ (that is, no wave in the radial direction), the solution, boundary condition, and dispersion relation are given by

$$\begin{aligned} \zeta_{n0} &= J_0(\kappa_{n0}r)e^{-i\sigma_{0n}t}, & (34)\\ J_0'(\kappa_{n0}a) &= 0, & (35)\\ \sigma_{n0}^2 &= gD_0\kappa_{n0}^2. & (36) \end{aligned}$$

The boundary condition given by (35) again fixes κ_{n0}, with an ascending sequence of positive eigenfrequencies following. This case is just like the case of no rotation ($f_0 = 0$), except that particle paths will now no longer be radial. For $s \neq 0$, substituting the dispersion relation given by (33) into (32) gives

$$-i\sigma\kappa_{ns}J_s'(\kappa_{ns}a) = \frac{f_0 is}{a}J_s(\kappa_{ns}a) = 0, \tag{37}$$

which fixes κ_{ns}. Solving (37) for σ and substituting (33), we have

$$\frac{sJ_s(\kappa a)}{\kappa a J_s'(\kappa a)} = \pm\sqrt{1 + \frac{(\kappa a)^2}{\beta}}, \tag{38}$$

where

$$\beta := \frac{f_0^2 a^2}{gD_0} \tag{39}$$

is called the Lamb Parameter.

Solutions admitted by this problem are given by the roots of (38), as illustrated in figure 4. For a given s, and $f_0 \to 0$ (and, consequently, $\beta \to 0$) the roots are given by $(\kappa a)^2 > 0$ pairs near the $J_s'(\kappa a) = 0$ line. As f_0 and β increase, $(\kappa a)^2$ pairs move farther apart, and a new root appears, with $(\kappa a)^2 < 0$. For this case, κ, and therefore the argument of the Bessel function in (23) will be an imaginary number. The radial part of the solution is then given by a modified Bessel function,

$$I_s(\kappa r) = i^{-n}J_n(ix) = e^{-n\pi i/2}J_n(xe^{i\pi/2}), \tag{40}$$

which decays away from the boundary. Figure 3 shows the dispersion relation given in (33) for a fixed s and different n. The pairs of eigenfrequencies corresponding to the κa pairs in figure 4 can be readily seen; they are gravity waves propagating in opposite directions. The $(\kappa a)^2 < 0$ mode is the Kelvin Wave.

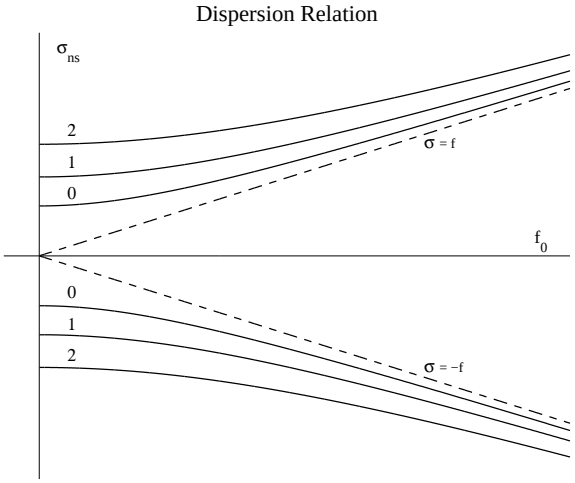

Figure 3: The dispersion relation (33) for different values of n. The Kelvin modes are shown by the dashed line.

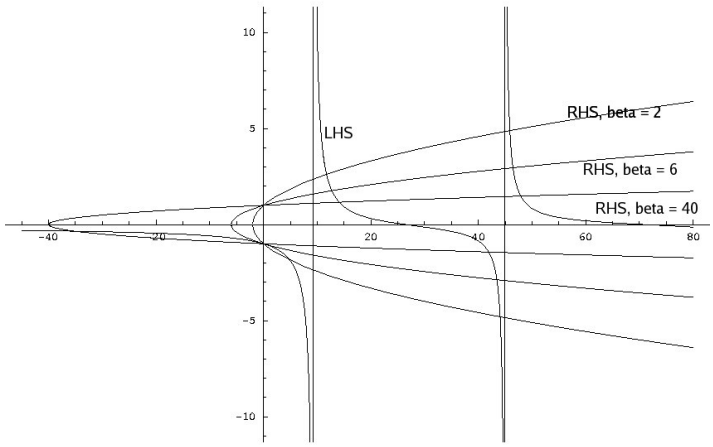

Figure 4: Illustration of the roots of (38). The curves opening to the right correspond to the right hand side of (38) for different β (with β increasing for tighter curves. The asymptotic function is the left hand side of (38). For this case, $s = 2$.

4 Rossby Modes

4.1 Linear Models for Rossby Waves

We now return to the Rossby modes. As discussed earlier, these are the low frequency solutions of the LTE in plane coordinates. Now defining the vorticity, ξ, in the usual way, i.e.

$$\xi = v_x - u_y, \tag{41}$$

we rewrite the shallow water wave equations to give

$$\frac{D}{Dt}\left(\frac{\xi + f}{D}\right) = 0, \tag{42}$$

where D/Dt is the material derivative, i.e.

$$\frac{D}{Dt} = \frac{\partial}{\partial t} + u\frac{\partial}{\partial x} + v\frac{\partial}{\partial y}.$$

Recalling that $f = f_0 + \beta y$ and $D = D_0 + \zeta$ we linearize (42) with respect to ξ, ζ, u and v to find an equation for the time evolution of the vorticity.

$$\begin{aligned}\frac{D}{Dt}\left(\frac{\xi + f}{D}\right) &= \frac{D}{Dt}\left(\frac{\xi + f_0 + \beta y}{D_0} - \frac{(f_0 + \beta y)\,\zeta}{D_0^2}\right) \\ &= \frac{\xi_t}{D_0} - \frac{f_0\zeta_t}{D_0^2} + \frac{\beta v}{D_0},\end{aligned} \tag{43}$$

where we have assumed that $\beta y \ll f_0$ to neglect the term proportional to $\beta y\zeta$.

Since Rossby waves are low frequency waves, $u_t \ll f_0 v$ and $v_t \ll f_0 u$ so that

$$-f_0 v \approx -g\zeta_x \quad f_0 u \approx -g\zeta_y. \tag{44}$$

Substituting (44) into (43), we find that we can rewrite (43)

$$\frac{g}{f_0 D_0}\left(\zeta_{xx} + \zeta_{yy}\right) - \frac{f_0}{D_0^2}\zeta_t + \frac{\beta g}{f_0 D_0}\zeta_x = 0. \tag{45}$$

Multiplying (45) through by $f_0 D_0/g$ (45) becomes

$$\nabla^2\zeta_t - \left(\frac{f_0^2}{gD_0}\right)\zeta_t + \beta\zeta_x = 0. \tag{46}$$

By considering the boundary condition on the coast, we can further simplify the vorticity equation for Rossby waves. As in the earlier discussion of gravity waves, at the coast we must have

$$\mathbf{u}\cdot\hat{\mathbf{n}} = 0,$$

so that if we define a local coordinate system at each point on the coast with the $\hat{\mathbf{s}}$ direction tangent to the coast, we must have $\zeta_s = 0$ so that

$$\zeta_{coast} = \Gamma(t), \tag{47}$$

i.e. that value of ζ is the same everywhere on the coast though it may be allowed to vary in time. For sufficiently short waves,

$$\nabla^2 \zeta_t \gg \left(\frac{f_0^2}{g D_0} \zeta_t \right), \tag{48}$$

so that to leading order (46) becomes

$$\nabla^2 \zeta_t + \beta \zeta_x = 0. \tag{49}$$

Since the boundary condition is independent of space, the time dependent boundary condition can, to leading order, be absorbed into ζ, so that (49) can be solved under the condition

$$\zeta_{coast} = 0. \tag{50}$$

4.2 Rossby Waves in a Square Basin

Suppose that ζ is periodic in time with frequency σ. That is, suppose that ζ can be written in the form

$$\zeta(x, y, t) = \Re \left\{ e^{-i\sigma t} \Phi(x, y) \right\}. \tag{51}$$

Substituting this expression for ζ into (49), we find that Φ satisfies the following boundary value problem.

$$\nabla^2 \Phi + \frac{i\beta}{\sigma} \frac{\partial \Phi}{\partial x} = 0, \quad \Phi_{coast} = 0. \tag{52}$$

To remove the x-derivative from (52) we further substitute

$$\Phi = e^{-i\beta x / 2\sigma} \phi(x, y) \tag{53}$$

into equation 52 we find that ϕ satisfies the boundary value problem

$$\nabla^2 \phi + \lambda^2 \phi = 0, \phi_{coast} = 0, \tag{54}$$

where $\lambda^2 = \beta^2 / 4\sigma^2$.

Consider Rossby waves in the rectangular basin $0 \leq x \leq x_0$, $0 \leq y \leq y_0$. Using separation of variables, we write

$$\phi(x, y) = X(x) Y(y) \tag{55}$$

and see that X and Y both satisfy equations for the harmonic oscillator. Therefore the boundary conditions imply that any function of the form

$$\phi = \phi_{mn} = \sin \frac{m\pi x}{x_0} \sin \frac{n\pi y}{y_0}, \tag{56}$$

with m, n positive integers, satisfies the boundary value problem and that σ is the corresponding eigenvalue,

$$\sigma = \sigma_{mn} = -\frac{\beta}{2\pi} \frac{1}{\left[\left(m^2 / x_0^2 \right) + \left(n^2 / y_0^2 \right) \right]^{1/2}}. \tag{57}$$

Note that the highest frequency modes are the ones with the smallest values of m and n. Substituting, our solution for ϕ_{nn} into (53) and subsequently into (51), we find that for each normal mode

$$\zeta = \cos\left[\frac{\beta x}{2\sigma_{mn}} + \sigma_{mn} t\right] \sin\left(m\pi \frac{x}{x_0}\right) \sin\left(n\pi \frac{y}{y_0}\right). \tag{58}$$

This solution consists of a carrier wave moving to the left modulated by sine function serving to satisfy the boundary conditions. The sine functions also create stationary nodes while the cosine function creates nodes which move to the left.

4.3 Circular Basin

Now suppose we have a circular basin with radius a. The definitions for ϕ follow exactly the same as for the square basin leaving the boundary value problem

$$\nabla^2 \phi + \lambda^2 \phi = 0, \quad \phi\,(r = a) = 0, \tag{59}$$

with $\lambda^2 = \beta^2/4\sigma^2$.

We again use separation of variables to write

$$\phi = R\,(r)\,\Theta\,(\theta) \tag{60}$$

to find that Θ and R satisfy the harmonic oscillator and Bessel Equations respectively. Therefore, the boundary conditions and single-valuedness imply that any function of the form

$$\phi = \phi_{nm} = \cos\,(m\theta + \alpha)\, J_m\,(k_{nm} r)\,, \tag{61}$$

with α an arbitrary phase angle, satisfies the boundary conditions under the conditions that m is a positive integer, J_m is the Bessel Function of order m, and

$$\xi_{mn} = k_{nm} a \tag{62}$$

is the n^{th} zero of the Bessel function of order m. The eigenvalue for σ is then

$$\sigma_{mn} = -\frac{\beta}{k_{nm}^2 a^2}, \tag{63}$$

and the corresponding eigenfunction is

$$\zeta_{mn} = \cos\left[\frac{\beta x}{2\sigma_{mn}} + \sigma_{mn} t\right] \cos\,(m\theta + \alpha)\, J_m\,(k_{nm} r)\,. \tag{64}$$

Therefore these eigenfunctions also represent a carrier wave moving to the left creating moving nodes modulated by an envelope of functions which create stationary nodes. In this case the stationary modes are radial lines corresponding to zeros of $\cos\,(m\theta + \alpha)$ and circles corresponding to zeros of $J_m\,(k_{nm} r)$.

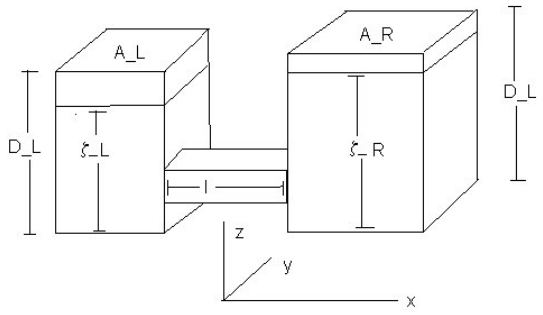

Figure 5: The Helmholtz Oscillator

5 Helmholz "Mass Exchange" Mode

We can solve for an additional normal mode, where fluid moves between two basins. The problem is illustrated in Fig. 5 in which A_L, D_L and A_R, D_R represent the cross-sectional area and depth of the left and right basins respectively. We further take l, w, and d to be the length, width, and depth of the connecting channel.

If we take $D_L, D_R \gg d$ so that the fluid height, ζ, in each basin can be taken as virtually constant within the basin and the connecting channel is always full. Define ζ_L and ζ_R as the time dependent fluid heights in the left and right basins, respectively. The total fluid volume in the system is

$$V = A_L\zeta_L + A_R\zeta_R + lwd \tag{65}$$

and must be conserved conserved. Differentiating (65) with respect to time, we derive the volume conservation equation:

$$A_L\left(\zeta_L\right)_t + A_R\left(\zeta_R\right)_t = 0. \tag{66}$$

Since we have taken ζ_L and ζ_R to be independent of space, we can express the time rate of change of the volume flux into the right basin as

$$\frac{d}{dt}A_R\left(\zeta_R\right)_t = A_R\left(\zeta_R\right)_{tt}.$$

Any fluid that enters the right basin must enter through the connecting channel. If we assume the velocity of the fluid in the channel is entirely in the lengthwise direction, then the fluid flux into the right basin is uwd, where u is the fluid velocity in the lengthwise direction and taken to be parallel to the x-axis. Therefore, equating the time rate of change of fluid into the right basin gives us

$$A_R\left(\zeta_R\right)_{tt} = u_t wd. \tag{67}$$

Since we have assumed that the flow in the channel is uniform and unidirectional, the momentum equation in the channel is $u_t = -g\zeta_x$. At the left edge of the channel, $\zeta = \zeta_L$

while $\zeta = \zeta_R$ at the right edge. Therefore, since the length of the channel is l, $\zeta_x \approx (\zeta_R - \zeta_L)/l$. Therefore, we can rewrite (67) as

$$A_R (\zeta_R)_t \, t \approx -wdg \frac{\zeta_R - \zeta_L}{l}. \tag{68}$$

Solving (65) for ζ_L and substituting into (68) we find that ζ_R satisfies the equation for a simple harmonic oscillator. That is

$$(\zeta_R)_{tt} + gwd \left(\frac{1}{A_R} + \frac{1}{A_L} \right) \zeta_R = K, \tag{69}$$

where K is a constant. This equation implies that the Helmholtz mass exchange mode does represent a simple wave solution of the shallow water wave equations with

$$\omega^2_{Helmholtz} = gwd \left(\frac{1}{A_R} + \frac{1}{A_L} \right). \tag{70}$$

6 Platzman's Analysis

Platzman et al. [1] computed approximate normal modes of the world oceans by computing the normal modes in the 8 to 80-hour spectrum of a numerical model of the LTE. Platzman's analysis focuses on large-scale features of the direct response of the deep ocean to the tidal potential, rather than coastal tides. The discretization of the model makes it an eigenvalue problem with 2042 total degrees of freedom. The eigenvectors have the form

$$(\xi, \phi, \psi) = Re[(Z, \Phi, \Psi) e^{i\sigma t}], \tag{71}$$

where σ is the eigenfrequency, ξ is the free surface elevation, ϕ is velocity potential, and ψ is the volume streamfunction.

Platzman et al. visualized the different normal mode motions described in the previous sections, by contouring the amplitude and phase of the mean elevation, as well as the energy density and flux, over the model grid. It is instructive to examine some example maps, which illustrate different normal modes.

Figure 6 shows a sample analysis from Platzman et al., of a topographic vorticity wave, as contained by the 14th computed normal mode, which has a period of $T = 33h$. The height contour plot in this figure (left panel) shows a sort of height "dome", and the phase lines (perpendicular to the lines of height) show the counterclockwise rotation about an amphidrome where the phase contours are anchored. The energy diagram (right panel) shows that energy is transported in an anticyclonic gyre, with the energy flow largely parallel to the phase velocity of the wave. (Since the study only looked for modes with periods between 8 and 80 hours, it couldn't clearly resolve any planetary vorticity waves.)

Similarly, Mode 12 (Fig. 7) can be understood, given the height and energy contours as the Helmholtz resonator mode described in section 5. The energy diagram for this mode shows a nearly uniform phase across each ocean, and the elevation contours could perhaps be interpreted as having a "node-like band" at the junction between the two oceans. A clearer argument for the Helmholtz resonator analogy is given by Fig. 8, which simply

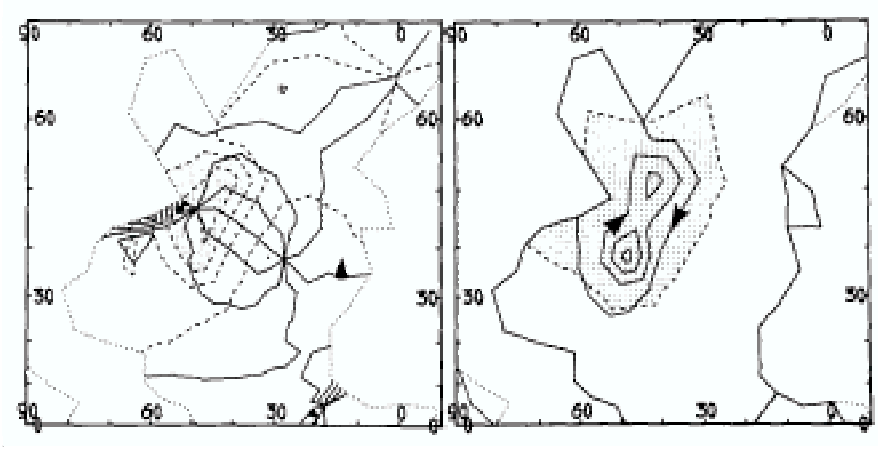

Figure 6: Platzman et al.'s computed mode 14, a vorticity wave near Newfoundland. Elevation is contoured in the left panel, total energy density on the right. Arrows are placed on the contour of zero phase, and point in the direction of phase propagation.

shows a polar plot of the amplitude and phase of the fluctuations in regional volume which are induced by that particular mode.

This figure suggests that the volume of the Arctic and North Atlantic oceans are in balance with the Indian and South Atlantic Oceans.

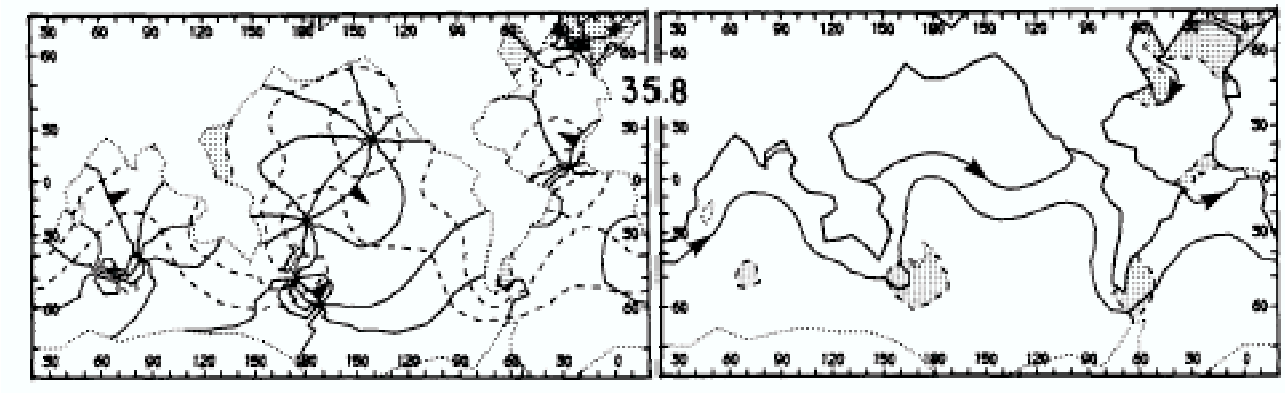

Figure 7: Platzman et al.'s computed mode 12, which can be interpreted as a Helmholtz resonator mode.

Mode 12 carries less than 30% rotational kinetic energy. Mode 15 (Fig. 9) also carries little rotational energy, though it also has a clear Kelvin Wave component in the southern ocean, with phase lines parallel to the coast of Antarctica, and eastward energy propagation.

As for gravity modes (Section 3), Platzman et al.'s model resolves 5 slow ($T < 24h$) gravity modes, but these tend to take on the appearance of vortical modes in the presence

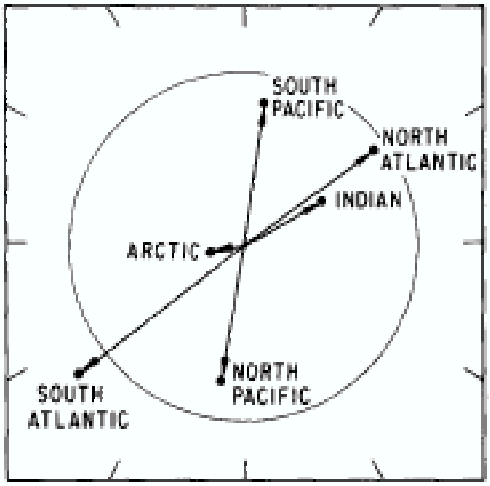

Figure 8: Volume-fluctuation vectors for Platzman et al.'s mode 12.

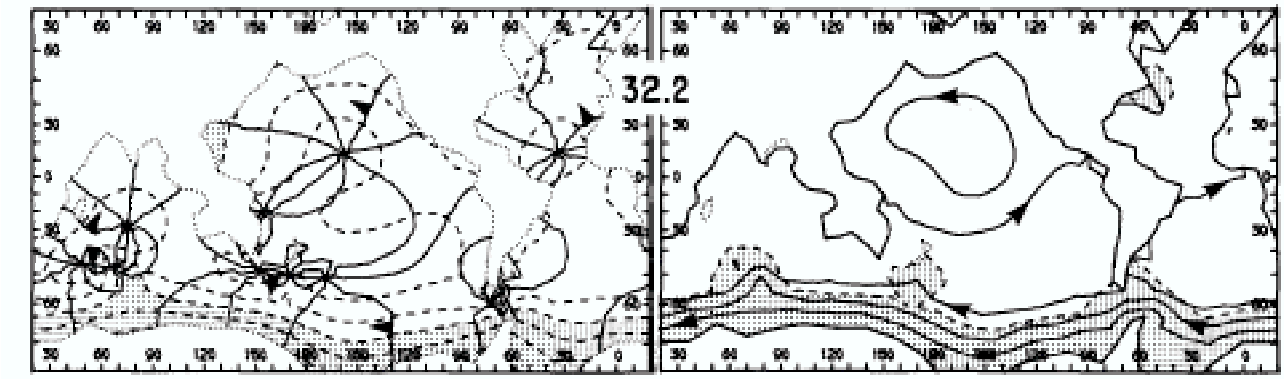

Figure 9: Platzman et al.'s computed mode 15, which contains a Kelvin Wave component.

of bottom topography. An example of a fast gravity wave is shown in figure 10, of mode 28. In this example, the arctic ocean seems to be strongly excited, and the arctic energy density is much larger than the global average.

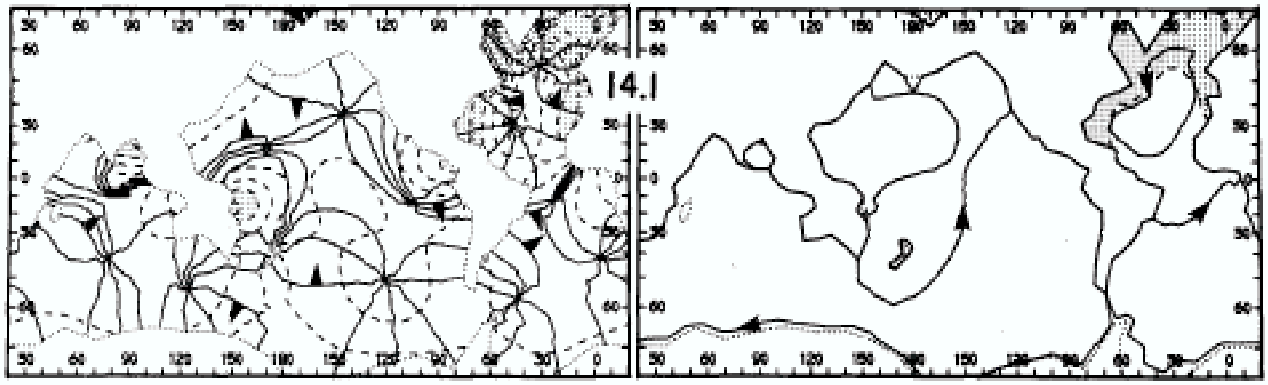

Figure 10: Platzman et al.'s computed mode 28, a gravity wave.

7 Resonance

The response of the oceans to tidal forcing at frequency ω, given a spectrum of ocean normal modes, can be written as

$$\zeta(\mathbf{x},t) = \mathbf{Re}\sum_n \frac{B_n(\omega)}{\omega_n - \omega - \frac{1}{2}iQ_n^{-1}\omega_n} S_n(\mathbf{x})e^{-i\omega t}, \tag{72}$$

where ω_n is the frequency of the nth normal mode of the oceans, $S_n(\mathbf{x})$ is the corresponding eigenfunction, and $B_n(\omega)$ is a complex factor that needs to be somehow determined. Q_n is a dissipation factor; that is, the nth normal mode dissipates a fraction $2\pi Q_n^{-1}$ of its energy per cycle. The response function given in equation (72) assumes that the functions $S_n(\mathbf{x})$ form a complete set. Equation (72) also makes the implicit assumption that the normal modes are linear waves. This assumption does not really hold in shallow water, where the nonlinear friction terms become significant. It is instructive to examine equation (72) for a hypothetical case where one mode (say,the zeroth mode) dominates, and its corresponding spatial response is constant, such that $B_0(\omega)S_0(\mathbf{x}) = C_0$. Then we can write

$$Ae^{i\Theta} = \frac{C_0}{\omega_0 - \omega - \frac{1}{2}iQ^{-1}\omega_0}. \tag{73}$$

This response function is plotted in figure 11. The age of the tide (i.e. the time lag between the tidal potential and the maximum of the response) can be found from $d\Theta/d\omega$, which, in this simple case, is given by

$$\frac{d\Theta}{d\omega} = \frac{\frac{1}{2}Q_0^{-1}\omega_0}{(\omega_0 - \omega)^2 + (\frac{1}{2}Q_0^{-1}\omega_0)^2}. \tag{74}$$

For the single-mode case, the maximum value is $2Q_0/\omega_0$ (at $\omega = \omega_0$). If the tide were dominated by single ocean mode, the age of the tide would be positive, and the same everywhere. Since

$$Q_0 \geq \frac{1}{2}\omega_0 \frac{d\Theta}{d\omega} \tag{75}$$

the age of the tide would put a lower limit on the quality factor Q_0.

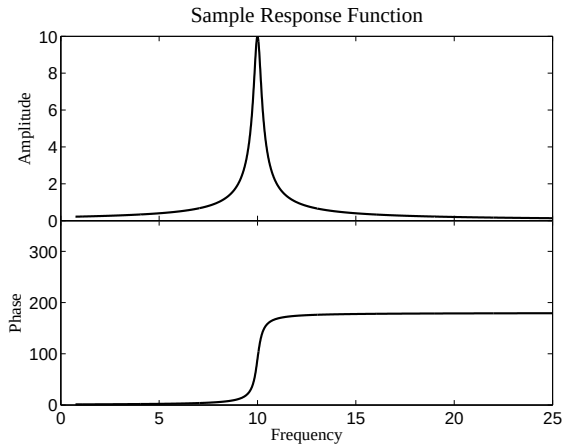

Figure 11: Sample response function for a single normal mode, where we have chosen $w_0 = 1$, $Q_0 = 25$, and $C_0 = 1$.

8 Comments on Inferences drawn from Ocean Models

Looking at the models for the ocean's normal modes we have just discussed, we can draw some interesting conclusions. Taking the dynamical solution of the "time scale" problem for the lunar orbit evolution as being solved by Hansen [2], Webb [3], Ooe et al. [4], and Kagan and Maslova [5], the models generate significantly smaller torques in the past than that implied by earth's present rotation rate. Platzman's work explains that the ocean has many different normal modes, some of which have frequencies close to the main tidal spectral lines. The modes grow more complex as frequency increases. In the past, the Earth's faster rotation forced tidal frequencies higher so that the modes with near-tidal frequencies were less well matched spatially to the large-scale tidal forcing, so that they were less easily excited. Therefore the torques were smaller since the tidal admittance to the tidal potential was also decreased from its current day value.

9 Why Ocean Tides are Back in Fashion

The LTE were written down 1776, so why are we still studying tides in 2004? There are several reasons: understanding why certain places see such large tides, understanding tidal dissipation from internal tide mixing, and the possibility of using the tides as a renewable energy source. We will discuss the first of these in this lecture.

Name	Type	Period(h)	Amp.
Q_1	L	26.87	0.0641
O_1	L	25.82	0.3800
P_1	S	24.07	0.2011
K_1	L/S	23.93	0.6392
N_2	L	12.66	0.0880
M_2	L	12.42	0.3774
S_2	S	12.00	0.1089

Table 1: Dominant constituents at Victora

10 The Tides at Victoria

If the moon were perfectly aligned with the equator, its motion would only cause semi diurnal tides. However, the moon orbits the earth at a declination angle which means that it also forces a diurnal tide. The dominant semi diurnal and diurnal tides at Victoria, BC, can be seen in Table 1.

The interactions of these tides account for the daily variations in the tides. M_2 and S_2 beat over the spring/neap cycle. K_1 and O_1 beat over a lunar month to allow for changes in the moon's declination which modulates the lunar diurnal tide. K_1 and P_1 beat over a year to allow for changes in the sun's declination which accounts for changes in the solar diurnal tide. Furthermore, M_2 and N_2 beat to provide a correction allowing for ellipticity in the moon's orbit which also effects the lunar diurnal tide.

Since K_1 has the largest amplitude we expect the tides in Victoria to look mostly diurnal. That is there should be approximately one maximum and one minimum tide during the day with some variations due to the other tides. However, in the third week of March 2004, for example, there were several consecutive days where there are two distinct maxima and minima. This is an example of the beating discussed in the previous paragraph. At the spring perigee, the sun and the moon were very close to the equatorial plane which diminishes the diurnals allowing the semidiurnals to appear more prominently, particularly at spring tides.

11 The World's Highest Tides

Two Canadian locations have recently both claimed that they have the world's largest tides. In the upper part of the Bay of Fundy, the tides rise up to 17m. Ungava Bay in Quebec also has tides that can reach at least 16.8m. Both of these maxima occur in an 18.61 year nodal cycle.

There have been several "explanations" offered by various sources for why the tides in the Bay of Fundy are so large. These include the idea that the Bay of Fundy is the closest point to the moon at these times and the belief that large tidal currents from the Indian Ocean can enter the bay because it opens to the south! In actuality, these large tides are more likely connected to a resonance phenomenon [6], which will be discussed in the next section.

12 Friction and Resonance

The time lag between the spring/neap cycles of the different tidal potential constituents, and the actual observed response of the oceans, is called the age of the tide [7]. It can be explained mathematically in terms of the response function given in (72) introduced in Section 7. The effect of friction can be examined more closely by approximating the energy dissipated due to friction, which is proportional to $u|u|$. If we assume that the tidal current u is the sum of a primary tidal constituent and a secondary, weaker one,

$$u = u_0(\cos\omega_1 t + \epsilon\cos\omega_2 t), \tag{76}$$

(where ϵ is a small parameter) then it can be shown that

$$u|u| = \frac{8}{3\pi}u_0^2(\cos\omega_1 t + \frac{3}{2}\cos\omega_2 t + ...), \tag{77}$$

where we have neglected higher-order harmonics. The 3/2 coefficient in the second term of (77) shows that the weaker tide feels a stronger frictional effect. In other words, the Q factor for the weaker tide will be 2/3 that of the stronger tide.

The response of the Bay of Fundy and the Gulf of Maine implies a resonant period of about 13.3 hours and a Q, for M_2, of about 5. On the west coast, the tidal response of the Strait of Georgia and Puget Sound can be modeled as a Helmholtz Resonance, where the tidal current enters a bay of surface area A through a channel of length L and cross section E. We will assume that the bay is small enough such that the height of the water surface rises uniformly everywhere. If the tide outside the bay is $a\cos\omega t$, the level inside is $\mathbf{Re}(a'e^{-i\omega t})$, where a' is the response amplitude in the bay. The current in the entrance channel is $\mathbf{Re}(ue^{-i\omega t})$. The continuity equation is is then

$$-i\omega a'A = Eu. \tag{78}$$

The channel dynamics are a balance between acceleration, friction, and the pressure gradient. The momentum equation can be written as

$$-i\omega u + g(a' - a)/L = -\lambda u, \tag{79}$$

where λ is simply a linear damping factor. As shown in equation (77), λ will be 50% larger for the constituents with weaker currents than the dominant M_2. The response in the bay will then be given by

$$a' = \frac{a}{1 - \frac{w^2}{w_0^2} - \frac{i\omega\lambda}{w_0^2}}, \tag{80}$$

where $\omega_0 = (\frac{gE}{AL})^{1/2}$ is the resonant frequency.

The frequency dependent response curve for a Helmholtz resonator given in equation (80). The response for a rectangular bay (not shown) can also be fitted to the data, that is, the tidal constituent frequencies and the corresponding amplitude and phase lag measurements.

For both cases, it seems that the observed tides straddle a resonant frequency ω_0, with $Q = \omega_0/\lambda$. For both cases, the fit returns a $Q \simeq 2$, which is low (and thus corresponds to high friction). This seems to be consistent with the high friction required by numerical models.

13 Nodal Modulation

The effect of the nodal modulation of the tide (due to the variation of the moon's declination) can be similarly written as a response curve, proportional to

$$a \propto \frac{a_0(1+\epsilon)}{1-\frac{\omega}{\omega_0}+\frac{1}{2}iQ_0^{-1}\frac{a}{a_0}}, \tag{81}$$

where the $1+\epsilon$ factor includes the effect of the modulation of semidiurnal forcing and the multiplier in the friction term allows for quadratic friction [8].

Away from resonance, the friction term becomes insignificant, and $a \propto 1+\epsilon$. Near resonance, however, the friction term becomes important, and $a \propto 1+\frac{1}{2}\epsilon$. Indeed, the actual modulation in the Bay of Fundy is less than in other areas.

Notes by David Vener and Lisa Neef

References

[1] G. Platzman, G. Curtis, K. Hansen, and R. Slater, "Normal modes of the world ocean. part ii: Description of modes in the period range 8 to 80 hours," J. Phys. Ocean. **11**, 579 (1981).

[2] K. Hansen, "Secular effects of oceanic tidal dissipation on the moon's orbit and the earth's rotation," Review of Geophysics **20**, 457 (1982).

[3] D. Webb, "Tides and the evolution of the earth moon system," Geophys. J. Roy. Astr. Soc. **70**, 261 (1982).

[4] H. S. M. Ooe and H. Kinoshita, "Effects of the tidal dissipation on the moon's orbit and the earth's ratation," Geophysical Monograph **59**, 51 (1990).

[5] B. Kagan and N. Maslova, "A stochastic model of the earth-moon tidal evolution accounting for the cyclic variations of resonant properties of the ocean: An asymptotic solution," Earth, Moon and Planets **66**, 173 (1994).

[6] C. Garrett, "Tidal resonance in the bay of fundy," Nature **238**, 441 (1972).

[7] C. Garrett and W. Munk, "The age of the tide and the 'Q' of the oceans.," Deep-Sea Res. **18**, 493 (1971).

[8] L. Ku, D. Greenberg, C. Garrett, and F. Dobson, "The nodal modulation of the m_2 tide in the bay of fundy and gulf of maine," Science **230**, 69 (1985).